Dear Reviewer,

Thank you for giving us the opportunity of a reply. We hope that we have satisfactorily addressed all queries.

Best regards

Pierre Sicard

Anonymous Referee #2

The specific methodological queries have largely been addressed, although in the revised text the authors have now introduced new lack of clarity in how they assigned particular IO3 values to each model grid square.

In L160 it is stated that vegetation was grouped into the three categories of 'conifer', 'crops' and 'deciduous trees.' What are tropical rain forests classified as? What are grasslands and dry shrub classified as? These don't seem to map readily onto the three specified vegetation classifications.

R - In this study, we have considered tropical forests and shrubs as deciduous trees while grassland was classified as cropland, similar to Sitch et al. (2007), as we have clarified this point in the text.

Even, Dynamic Global Vegetation Models make use of plant functional type rather than complex and specific vegetation to simulate shifts in potential vegetation as a response to shifts in climate. In Sitch et al (2007), data from field observation were used to calibrate plant-ozone effects for the five plant functional types described by MOSES land-surface scheme (Broadleaf trees, Needleleaf trees, C3 Grass, C4 Grass & Shrub).

I am also not clear how a % change in IO3 can be derived if the AOT40 value in a particular grid square was initially zero (L425). An IO3 value may become non-zero in a new scenario, where previously it was zero, but it is not possible to assign a % change to a change from zero.

R – The percentage of change is computed as following: [(RCPx - hist) / hist] * 100

Clearly if the AOT40 during the historical period is 0 then the percentage of change is undefined and therefore we have considered and set these grid points as missing values, as we will now state in the text. For example, readers can see there is no color in Figure 3 for the CESM-CAM model in South America (Venezuela coast) because we have an abrupt change in AOT40 between the historical run (AOT40 was 0) and RCP8.5 projections (Figure 2).

Whilst the authors may have presented a lot of careful and numerically-correct calculations, I still wonder whether the use of various 'globally-wide' approximations means that one has to be very cautious about taking the results, particularly for changes in IO3, too literally. Example of these 'global' approximations include the calculation of AOT40 values from 08.00 to 20.00 everywhere globally regardless of latitude and time of year, the calculation of AOT40 for a full-year, and the assignment of all global vegetation to just 3 vegetation classes. The authors have responded that because they are interested in examining relative changes in impacts on vegetation these issues are not so important, but surely if growing season length (and extent of daylight hours) at a particular location is relevant for ozone-induced injury

then how the annual distributions of ozone concentrations change in the future under different scenarios (and also how growing seasons change under different scenarios) will have a quantitative impact on the extent of ozone-induced injury in the real world compared to these modelled worlds.

R – The current chemistry models cannot predict changes in phenology, thus the growing season length is the same between the historical period and different RCPs. Here, we applied the same approximation of ACCMIP models. However, a note of caution including a citation to the phenological issue (Anav et al., 2017) will be included in the discussion.

Plant phenology plays a pivotal role in the climate system as it regulates the gas exchange between the biosphere and the atmosphere. Currently, in many risk assessment studies, the phenology function is based on a simple latitude and topography model. The Chemistry Models do not take into account the shifts in plant phenology and in start and end date of the growing season, however a first attempt to study the role of phenology on stomatal ozone uptake is shown by Anav et al (2017).

Much of the conclusions section remains more like general discussion (particularly in its extensive reference to prior literature) than 'take home' conclusions for the reader.

R – The section "conclusions" was shortened and a few references were moved towards the section "discussion" or removed.

There are also a few issues with some of the text in this section: (i) the sentence in L529-530 is not a complete sentence; (ii) the statement in L548-549 that AOT40-based critical levels "will be exceeded over many areas…" is not clear: to which RCP scenario(s) is this sentence referring? It is also potentially a bit misleading because even though AOT40 may be exceeded in certain areas, actually for two of the three future scenarios investigated AOT40 values will be less exceeded in the future than in recent history; (iii) L569 refers to sensitivity of grasslands to ozone injury but yet the authors' methodology does not refer to how IO3 is calculated for grasslands.

R – All these issues were addressed.

Please explicitly state somewhere in the text that tabulated and quoted values of global, NH and SH mean surface ozone, AOT40, and IO3 are derived from averaging values over the global/NH/SH land areas only, not over their full respective geographic domains.

R – We agree to add an explicit statement in the reviewed version for tables 3. Lines 184-186, we have addressed this point by adding this statement.

Introduction

Tropospheric ozone (O_3) is a secondary air pollutant, i.e. it is not emitted as such in the air but it is formed by reactions among precursors (e.g. CH_4, VOCs, NOx). Ozone is an important greenhouse gas resulting in a direct radiative forcing of 0.35-0.37 W m^{-2} on climate (Shindell et al., 2009; Ainsworth et al., 2012). Despite significant control efforts and legislation to reduce O_3 precursor emissions, tropospheric O_3 pollution is still a major air quality issue over large regions of the globe (Lefohn et al., 2010; Langner et al., 2012; Young et al., 2013; Cooper et al., 2014; EEA, 2015; Sicard et al., 2016a,b; Ochoa-Hueso et al., 2017). Long-range transport of O_3 and its precursors can elevate the local and regional O_3 background concentrations (Ellingsen et al., 2008; Wilson et al., 2012; Paoletti et al., 2014; Derwent et al., 2015; Xing et al., 2015; Sicard et al., 2016a). Therefore, remote areas such as the Arctic region can be affected (Langner et al., 2012). The current surface O_3 levels (35-50 ppb in the northern hemisphere, NH) are high enough to damage both forests and crops by reducing growth rates and productivity (Wittig et al., 2009; Anav et al., 2011; Mills et al., 2011; Ashworth et al., 2013; Proietti et al., 2016).

Increasing atmospheric CO_2, nitrogen deposition and temperatures enhance plant growth, and increase primary production and greening of plants (Nemani et al., 2003; Zhu et al., 2016). At the global scale, a widespread increase of greening and net primary production (NPP) is observed over 25-50% of the vegetated area, while a decrease is observed over only 7% of the globe (Nemani et al., 2003; Zhu et al., 2016). In contrast, a previous modeling study over Europe shows how surface O_3 reduces the mean annual gross primary production (GPP) by about 22% and the leaf area index by 15-20% (Anav et al., 2011). Similarly, Proietti et al. (2016), using different *in-situ* measurements collected over 37 European forest sites, found a GPP decrease (up to 30%) caused by O_3 during the time period 2000-2010. At global scale, over the time period 1901-2100, GPP is projected to decrease by 14-23% (Sitch et al., 2007). As a consequence of reduced photosynthetic assimilation, the total biomass of trees is estimated to be decreased by 7% under the current ground-level O_3 mean concentrations (40 ppb on average) and by 17% at mean O_3 concentrations expected in 2100 (97 ppb based on a meta-analysis) compared to preindustrial O_3 levels in NH (about 10 ppb, Wittig et al., 2009). From experiments, Wittig et al. (2009) also reported that the total tree biomass of angiosperms was reduced by 23% at O_3 mean concentrations of 74 ppb, and by 7% at 92 ppb for gymnosperms. High surface O_3 levels, exceeding 40 ppb, do occur in many regions of the globe with associated economic costs of several billion dollars per year (Wang and Mauzerall,

2004; Ashmore, 2005). Ashworth et al. (2013) reported an annual loss of 3.5% for wheat (very O_3-sensitive) and 1.0% for maize (more O_3-tolerant) for Europe in 2010 relative to 2000, while Holland et al. (2006) estimated a €4.5 billion loss in the production of 23 common crop species, due to surface O_3 exposure by 2020 relative to 2000.

The international Tropospheric Ozone Assessment Report (TOAR) establishes a state-of-the-art of global O_3 metrics for climate change, human health and crop/ecosystem research (Lefohn et al., 2017). To assess the potential O_3 risk and protect vegetation from O_3, different metrics are used: the European and US standard (AOT40 and W126, respectively) are based on exposure-based metrics, while flux-based metrics have been introduced only recently (UNECE, 2010; Klingberg et al., 2014; EEA, 2015). Unlike the exposure-based metrics, which only rely on the surface O_3 concentration, the flux-based metrics were developed to quantify the accumulation of damaging O_3 taken up by vegetation through the stomata over a species-specific phenological time-window. These metrics also provide an information-rich tool in assessing the relative effectiveness of air pollution control strategies in lowering surface O_3 levels worldwide (Monks et al., 2015). By reducing plant photosynthesis and growth, high surface O_3 levels will result in reduction in carbon storage by vegetation, and finally an indirect radiative forcing as a consequence of the CO_2 rising in the atmosphere (Sitch et al., 2007; Ainsworth et al., 2012). This rising CO_2 reduces stomatal conductance which decreases O_3 flux into plants leading to increased O_3 levels in the air of 3-4 ppb during the growing season over the NH by doubling of CO_2 concentration (Fiscus et al., 2005; Sanderson et al., 2007).

Projected changes in ground-level O_3 vary considerably among models (Stevenson et al., 2006; Wild, 2007) and emission scenarios. In earlier studies, the emissions of O_3 precursors were based on a high population growth, leading to very high projected surface O_3 concentrations by 2100 (Stevenson et al., 2000; Zeng and Pyle, 2003; Shindell et al., 2006). The last emission scenarios, i.e. the Representative Concentration Pathways (RCPs) were developed as part of the Fifth Assessment Report of the Intergovernmental Panel on Climate Change (Meinshausen et al., 2011; van Vuuren et al., 2011; Cubasch et al., 2013; Myhre et al., 2013). These scenarios include e.g. different assumptions on climate, energy access policies, and land cover and land use changes (Arneth et al., 2008; Kawase et al., 2011; Kirtman et al., 2013). Until now, studies on O_3 pollution impacts on terrestrial ecosystems are either limited to a single model or to particular regions (e.g. Clifton et al., 2014; Rieder et al.,

2015) and only a few applications of global or regional models under the new RCPs scenarios were carried out (Kelly et al., 2012). In the framework of the Atmospheric Chemistry and Climate Model Intercomparison Project (ACCMIP), different simulations were performed by Lamarque et al. (2013) and Young et al. (2013) from 16 global chemistry models.

A few issues about surface O_3, such as a better understanding of spatial changes and a better assessment of O_3 impacts worldwide, are still challenging. To overcome these issues, the aim of this study is to quantify, for the first time, the spatial and temporal changes in the projected potential O_3 impacts on photosynthetic carbon assimilation of vegetation at global scale, by comparing the O_3 potential injury at present with that expected at the end of the 21st century from different global chemistry models. The purpose of this study is not to provide a quantitative estimation of the ecosystem injury due to O_3 but to highlight the world areas at higher risk and changes by 2100.

Materials and Methods

ACCMIP models and RCP scenarios

The global chemistry models used in this work were developed under the ACCMIP project. A detailed description of the selected models and of the emission scenarios (i.e. RCPs) is included in Supplementary Information (SI). ACCMIP models were widely validated and used to evaluate projected changes in atmospheric chemistry and air quality under different emission and climate assumptions (e.g. Lamarque et al., 2010; Fiore et al., 2012; Bowman et al., 2013; Lee et al., 2013; Voulgarakis et al., 2013). Lamarque et al. (2013) and Young et al. (2013) provided the main characteristics of 16 models and details for the ACCMIP simulations. Although within the ACCMIP project 16 models are available, due to the lack of hourly O_3 concentration here we only focus on 6 global chemistry models with different configurations (Table 1).

The length of historical and RCP simulations vary between models, but for all models the historical runs cover a period centered around 2000, while the time-slice of RCPs is centered around 2100 (Table 1). As for each model we compare the relative mean change between the historical and RCP simulations, a different length in the number of years used in the analysis does not affect the results.

Potential ozone injury on vegetation

The O_3 exposure-based index, i.e. AOT40 (ppb h), is a metric used to assess the potential O_3 risk to vegetation from local to global scales (Emberson et al., 2014). In literature, AOT40 is computed as sum of the hourly exceedances above 40 ppb, for hours between 8:00 hours and 20:00 hours or for hours with a solar radiation exceeding 50 Wm^{-2} over species-specific growing seasons (UNECE, 2010). Conventionally, two major growing-season time windows are used, i.e. six months (April to September) for temperate climates, e.g. in Europe and all-year round for Mediterranean, subtropical and tropical-type climates where vegetation is physiologically active all along the year (Paoletti et al., 2007).

UNECE (2010) supports the use of a growing season, but a fixed time-window does not allow incorporating the changes in the growing season due to climate change and would thus not be well suited when investigating changes over time. A recent study over Europe showed how computing AOT40 only over the growing season (i.e. April-September) would lead to an underestimation of AOT40 up to 50% for conifer trees, while in case of deciduous trees the underestimation is much smaller (< 5%, Anav et al., 2016). Besides, it should be noted that in Anav et al. (2016) the AOT40 is computed year-round. We computed the AOT40 for a model grid for hours between 8:00 hours and 20:00 hours (local time) for all days of the year. Therefore, we computed AOT40 as follows:

$$AOT40 = \int_{01\,jan}^{31\,dec} \int_{8am}^{8pm} \max(([O_3] - 40), 0).dt \qquad (1)$$

where $[O_3]$ is hourly O_3 concentration (ppb) simulated by the models at the lower model layer and *dt* is time step (1h). The function "maximum" ensures that only values exceeding 40 ppb are taken into account. For the protection of forests, a critical level of 5 ppm.h calculated over the growing season is recommended by UNECE (2010). Within the 2008/50/CE Directive, the critical level for agricultural crops (3ppm.h) is adopted as the long-term objective value for the protection of vegetation by 2020.

The current chemistry models cannot predict changes in phenology over time, thus the growing season length is the same between the historical period and different RCPs. The use of a common fixed time-window (8-20h) all year-round at global level allows skipping the use of a latitude model, which would increase the level of complexity and uncertainties.

Because the growing season is highly variable across the latitude, rather than introducing further uncertainties by using a latitude model to simulate the growing season, we applied here a simplified approach with a year-long growing season which should be considered as a worst case study. This approach is valuable and can be easily applied at global scale to compare the historical and projected potential risk to vegetation.

The O_3 concentration to be used in AOT40 calculation should be at the top of the canopy; however, most of models used here provide O_3 concentrations at 90-120 m. Nevertheless, even if the O_3 concentration is simulated at different elevations above the sea level, as for each model we compare the variation between present and future, the change is consistent because the elevation is the same. In case of risk assessment, by calculating AOT40 year-round, an overestimation can be observed over polluted region of NH. Since the aim of this study is to compare how O_3 stress to vegetation changes between historical period and future, even if the AOT40 is misestimated at a given model grid point, as we compared the changes in AOT40 at the same model grid point, the relative mean change is consistent.

From the AOT40, a factor of risk for forests and crops can be computed (Anav et al., 2011; Proietti et al., 2016). Thus, the potential O_3 impact on photosynthetic carbon assimilation (IO_3), in the worst-case scenario, is expressed through a dimensionless value as following:

$$IO3 = \alpha \times AOT40 \quad (2)$$

where α is an empirically derived O_3 response coefficient representing the proportional change in net photosynthesis per unit of AOT40 (Anav et al., 2011). From the Global Land Cover Facility (GLCF) data at 1° of spatial resolution, we grouped the vegetation in three categories: conifers, crops (including grassland) and deciduous (including tropical forests and shrubs) trees. Even, Dynamic Global Vegetation Models make use of plant functional types rather than complex and specific vegetation to simulate shifts in potential vegetation as a response to shifts in climate (Sitch et al., 2007). The relationships between cumulative ozone exposure and reductions in net photosynthesis vary among and even within species (Reich, 1987; Ollinger et al., 1997). Differences in response per unit uptake tend to be greater in magnitude between functional groups (e.g., hardwoods vs. conifers) where leaf structure and plant growth strategy differ most widely (Reich, 1987).The dimensionless coefficient for coniferous trees (0.7×10^{-6}) and crops (3.9×10^{-6}) are based on the regressions of the photosynthesis response to O_3 (Reich, 1987), while the coefficient for deciduous trees

(2.6×10^{-6}) is based on Ollinger et al. (1997). From simulated changes in the risk factor, we can highlight potential risk areas for vegetation.

Results and Discussion

Although differences in the simulated global O_3 spatial pattern were previously discussed and analyzed (e.g. Lamarque et al., 2013), we show the mean annual O_3 concentration at the lower model layer in Figure 1 because O_3 concentration explains AOT40 patterns. Then, in Figure 2 we show and discuss the AOT40 spatial and temporal distribution from the ACCMIP models for the historical and RCPs simulations, and finally in Figure 3 we show the percentage of variation of IO3, i.e. the change in the potential impact of O_3 on photosynthetic carbon assimilation for the ACCMIP models computed comparing the RCPs simulations with historical runs. All spatial averages were calculated over land surfaces. A detailed description of each figure, model by model, is included in Supplementary Information (SI).

Spatial pattern of historical ozone concentration and AOT40

The highest surface O_3 concentrations (Fig. 1) and potential O_3 impacts (Fig. 2) are found in the NH, highlighting a hemispheric asymmetry. The averaged values of global, NH and SH mean surface O_3, AOT40 and IO3 are derived from averaging values over the global/NH/SH land areas only (Tables 3). AOT40 was used widely during the last two decades, not only in Europe but also in South America (Moura et al., 2014) and Asia (Hoshika et al., 2011) when environmental factors are not limiting, e.g. water availability, air temperature, solar radiation affecting stomata opening (Anav et al., 2016; De Marco et al., 2016).

The multi-models O_3 mean concentration, averaged over the land points of the domain, is 37.9 ± 4.3 ppb in NH and 22.9 ± 3.8 ppb in SH (Table 3a). Over land surfaces, the NH extratropics (i.e. mid-latitudes beyond the tropics) has 65% more O_3 than the SH extratropics (data not shown). Similarly, the highest AOT40 values are found in the NH, with an averaged AOT40 of 24.8 ± 10.1 ppm.h in NH and 2.5 ± 1.7 ppm.h in SH (Table 3a).

According to previous studies, the annual mean background O_3 concentrations at NH mid-latitudes range between 35 and 50 ppb during the end of the 20th century (e.g. Cooper et al., 2012; IPCC, 2014; Lefohn et al., 2014). Similarly, we found historical surface O_3 mean concentrations ranging between 35 and 50 ppb and 35-50 ppm.h for AOT40 in the NH, with

the highest values occurring over Greenland and in the latitude band 15-45°N, particularly around the Mediterranean basin, Near East, Northern America and over the Tibetan plateau (> 50 ppb and 70 ppm.h) while the lowest O_3 burden (15-30 ppb, < 20 ppm.h) was recorded in SH, particularly over Amazon, African and Indonesian rainforests where the O_3 dry deposition rate is maximum, up to 1.80 cm s^{-1} for mixed wood forests (Wesely and Hicks, 2000). Tropospheric O_3 has a significant source from stratospheric O_3 (Parrish et al., 2012) and it can be transported by the large-scale Brewer-Dobson overturning circulation, i.e. an upward motion from the tropics and downward at higher latitudes, resulting in higher O_3 concentrations in the extratropics (Hudson et al., 2006; Seidel et al., 2008; Parrish et al., 2012). The six models are able to reproduce the spatial pattern of O_3 concentration and thus AOT40 worldwide.

The highest historical O_3 mean concentrations are observed in GFDL-AM3 and the lowest are found in MIROC-CHEM. In the early 2000s, the maximum global O_3 mean concentration (39 ppb) in GFDL-AM3 is associated to the lowest annual total NOx emissions (46.2 Tg, Table 2a) and low LNOx (4.4 Tg) while the minimum global O_3 mean concentration (28 ppb) in MIROC-CHEM is related to the highest emissions of total NOx per year (57.3 Tg) and erroneously high LNOx (9.7 Tg per year, Lamarque et al., 2013). MIROC-CHEM simulates 58 gaseous species in the chemical scheme with constant present-day biogenic VOCs emissions while GFDL-AM3 simulates 81 species (Stevenson et al., 2012; Lamarque et al., 2013). In GISS-E2-R, the hemispheric asymmetry in O_3 is more important with e.g. a mean concentration of 22 ppb in SH and 42 ppb in NH. A stronger global AOT40 mean (26 ppm.h) is observed in GISS-E2-R and the lowest (7 ppm.h) in MIROC-CHEM for historical simulations. Model-to-model differences are observed due to different natural emissions of O_3 precursors (e.g. lightning NOx) and the different chemical schemes used.

Higher O_3 burdens (mean concentration > 50 ppb, AOT40 >70 ppm.h) are simulated at high-elevation areas, e.g. at Rocky and Appalachian Mountains and over the Tibetan plateau (Fig. 1, Fig. 2).At high-elevation, solar radiation, biogenic VOC emission, exchange between free troposphere and boundary layer, and stratospheric O_3 intrusion within the troposphere are more important that at the surface layer (Steinbacher et al., 2004; Kulkarni et al., 2011; Lefohn et al., 2012). Altitude reduces the O_3 destruction by deposition and NO (Chevalier et al., 2007). In addition, due to the high elevation, ambient air remains colder and dryer in summer, leading to lower summertime O_3 losses from photolysis (Helmig et al., 2007). The

high-elevation areas, characterized by higher O_3 burdens, are well simulated in GISS-E2-R and MOCAGE models.

The Tibetan plateau, so-called "ozone valley", is the highest plateau in the world, with a mean height of 4000 m a.s.l. (Tian et al., 2008) with strong thermal and dynamic influences on regional and global climate (Chen et al., 2011). High surface O_3 mean concentrations (40-60 ppb) were reported in previous studies (e.g. Zhang et al., 2004; Bian et al., 2011; Guo et al., 2015; Wang et al., 2015). Although this region is remote, road traffic, biofuel energy source, coalmines and trash burning are prevalent. These pollution sources contribute to significant amount of NOx, CO and VOCs (Wang et al., 2015). The high O_3 levels are attributed to the combined effects of high-elevation surface, thermal and dynamical forcing of the Tibetan plateau and *in-situ* photochemical production in the air trapped in the plateau by surrounding mountains (Guo et al., 2015; Wang et al., 2015). The dynamic effect, associated with the large-scale circulation, is more important than the chemical effect (Tian et al., 2008; Liu et al., 2010) and responsible for the high O_3 levels over the Tibetan plateau. The six models are able to well reproduce the high surface O_3 mean concentrations (> 50 ppb) over the Tibetan plateau.

Higher O_3 mean concentrations (> 60 ppb) are also observed in Southwestern U.S., at the stations inland close to Los Angeles, in Northeastern U.S. and East Asia (e.g. Beijing) (Fig. 1). The American Southwest is an O_3 precursor hotspot where the industrial sources emit CH_4 and VOCs into the air (Jeričević et al., 2013) and the eastern and northern desert areas have higher ambient O_3 than urban areas of southern California due to four factors: on-shore winds, gasoline reformulation, eastward population expansion and nighttime air chemistry (Arbaugh and Bytnerowicz, 2003). The surface concentrations show higher O_3 levels in areas downwind of O_3 precursor sources, i.e. urban and well-industrialized areas, at distances of hundreds or even thousands of kilometers due to transport of O_3 and precursors, including "reservoir" species such as PAN, lower O_3 titration by NO and higher biogenic VOC emission (Wilson et al., 2012; Paoletti et al., 2014; Monks et al., 2015; Sicard et al., 2016a).The higher O_3 levels in areas downwind of O_3 precursor sources are well simulated in GISS-E2-R and MOCAGE models.

Over Greenland, mean O_3 concentrations during the historical runs, ranged from 40 to 55 ppb (Fig. 1) except in MIROC-CHEM (20-25 ppb). Similarly, Helmig et al. (2007) reported

annual mean of surface O_3 concentrations of 47 ppb over Greenland between 2000 and 2005, particularly at the high-elevation Summit station (3200 m a.s.l.). Several investigations of snow photochemical and oxidation processes over Greenland concluded that photochemical O_3 production can be attributed to high levels of reactive compounds (e.g. oxidized nitrogen species) present in the surface layer during the sunlit periods due to local sources e.g. NOx enhancement from snowpack emissions, peroxyacetyl nitrate (PAN) decomposition, boreal forest fires or ship emissions (Granier et al., 2006; Stohl et al., 2007; Legrand et al., 2009; Walker et al., 2012). PAN to NOx ratio increases with increasing altitude and latitude (Singh et al., 1992). The PAN reservoir for NOx may be responsible for the increase in surface O_3 concentrations at high latitudes (Singh et al., 1992). Local O_3 production does not appear to have an important contribution to the ambient high O_3 levels (Helmig et al., 2007), however the long-range O_3 transport can elevate the background concentrations measured at remote sites, e.g. Greenland (Ellingsen et al., 2008; Derwent et al., 2010). Low dry deposition rates for O_3, from 0.01-0.05 cm s^{-1} over oceans and snow, the downward transport of stratospheric O_3, the photochemical local production and the large-scale transport (Zhang et al., 2003; Legrand et al., 2009; Walker et al., 2012; Hess and Zbinden, 2013) are known factors to explain higher O_3 pollution over Greenland.

The surface O_3 concentrations (> 40 ppb) and AOT40 (> 60 ppm.h) are higher over deserts, downwind of O_3 precursor sources (e.g. Near East, Sierra Nevada, Colorado Desert), due to lower O_3 dry deposition fluxes (Wesely and Hicks, 2000), O_3 precursors long-range transport from urbanized areas and high insolation. Around the Mediterranean basin, elevated AOT40 values (> 60 ppm.h) are recorded, mainly due to the industrial development, road traffic increment, high insolation, sea/land breeze recirculation and O_3 transport (Sicard et al., 2013). All models, except MIROC-CHEM, are able to well reproduce the high surface O_3 mean concentrations over Greenland and over deserts.

Projected changes in ozone concentration and AOT40

Recent studies display a mean global increase in background O_3 concentration from a current level of 35-50 ppb (e.g. IPCC, 2014; Lefohn et al., 2014) to 55-65 ppb (e.g. Wittig et al., 2007) and up to 85 ppb at NH mid-latitudes by 2100 (IPCC, 2014). During the latter half of the 20th century surface O_3 concentrations have increased markedly at NH mid-latitudes (e.g. Oltmans et al., 2006; Parrish et al., 2012; Paoletti et al., 2014), mainly related to increasing anthropogenic precursor emissions related to economic growth of industrialized countries

(e.g. Lamarque et al., 2005). Our results indicate that the future projections of the mean surface O_3 concentrations and AOT40 vary considerably with the different scenarios and models (Fig. 1 and 2). The six models simulate a decrease of O_3 concentration by 2100 under the RCP2.6 and RCP4.5 scenarios, and an increase under the RCP8.5 scenario (Lamarque et al., 2011). In our study, the averaged relative changes in surface O_3 concentration means (and AOT40) for the different RCPs are: -21% (-75%) for RCP2.6, - 10% (-50%) for RCP4.5 and + 14% (+69%) for RCP8.5 with a strong disparity between both hemispheres, e.g. - 8% in SH and - 25% in NH for RCP2.6 (Tables 3b-c). RCP8.5 is the only scenario to show an increase in global background O_3 levels by 2100 (+ 23% in SH and + 11% in NH).

Under the RCP2.6 scenario, all models predict that surface O_3 will strongly decrease worldwide, except in Equatorial Africa where higher O_3 levels are observed in GFDL-AM3, GISS-E2-R and MOCAGE. In CESM-CAM, GFDL-AM3 and MIROC-CHEM, a homogeneous decrease in O_3 burden is simulated worldwide while in GISS-E2-R, MOCAGE and UM-CAM, the strongest decrease in surface O_3 mean concentrations are found where high historical O_3 concentrations were reported. Under RCP4.5 scenario, the surface O_3 mean concentrations and AOT40 values are lower than historical runs worldwide for all models except in MOCAGE where deterioration is observed over Canada, Greenland and East Asia. For all models, the surface O_3 levels and AOT40 are higher for RCP8.5 as compared to historical runs and the highest increases occur in the North-western America, Greenland, Mediterranean basin, Near East and East Asia. The AOT40 values, exceeding 70 ppm.h, are found over the Tibetan plateau and in Near East and over Greenland. For RCP8.5, GFDL-AM3 is the most pessimistic model and MIROC-CHEM the most optimistic. By the end of the 21st century, similar patterns are evident for RCP4.5 compared to RCP2.6 and RCP4.5 simulation is intermediate between RCP2.6 and RCP8.5 ones.

For all models and RCPs, the O_3 hot-spots (mean concentrations > 50 ppb and AOT40 > 70 ppm.h) are over Greenland and South Asia, in particular over the Tibetan plateau. The highest increases are observed in NH, in particular in North-western America, Greenland, Near East and South Asia (> 65 ppb). For the three RCPs, no significant change in ground-level O_3 is observed in SH and the SH extratropics makes a small contribution to the overall change.

A recent global study showed the geographical patterns of surface air temperature differences for late 21st century relative to the historical run (1986-2005) in all RCP scenarios (Nazarenko

et al., 2015).The global warming in the RCP2.6 scenario is 2-3 times smaller than RCP4.5 scenario and 4-5 times smaller than RCP8.5 scenario (Nazarenko et al., 2015). For the three RCPs, the greatest change is observed over the Arctic, above latitude 60°N, and in the latitude band 15-45°N (IPCC, 2014; Nazarenko et al., 2015). The least warming is simulated over the large area of the Southern Ocean. For RCP8.5 scenario, the global pattern of surface O_3 levels and AOT40 (Fig. 1-2) is similar to surface air temperature increase distribution. For RCP8.5, significant increases in air temperature are simulated over latitude 60°N and over the Tibetan plateau (more than 5°C). An increase of 4-5°C over the Near East, East and South Asia, North and South Africa and Canada are simulated as well as + 1-3°C for the rest of the world (Nazarenko et al., 2015). The tropospheric warming is stronger in the latitude band 15-45°N (Seidel et al., 2008) and Hudson et al. (2006) have demonstrated that O_3 trends over a 24-year period in the NH are due to trends in the relative area of the tropics and mid-latitudes and Polar Regions. ll models are able to reproduce the global pattern of air temperature changes distribution in agreement with surface O_3 concentrations changes.

The spread in precursor emissions (e.g. VOCs, NOx, CO) is due to the range of representation of biogenic emissions (NOx from soils and lightning, CO from oceans and vegetation) as well as the complexity of chemical schemes in particular for NMVOCs simulations (e.g. isoprene) from explicitly specified to fully interactive with climate. RCP2.6 scenario has the lowest O_3 precursor concentrations, and RCP8.5 has relatively low NOx, CO and VOCs emissions, but very high CH_4 (Table 2b). The global emissions of NOx (-44%), VOCs (-5%) CO (-40%) and CH_4 burden (-27%) decline, while LNOx increase by e.g. 7% under RCP2.6 (Table 2b). The CO (-32%) and NOx (-20%) emissions have decreased while LNOX (+33%), VOCS (+1%) and CH_4 burden have increased (+120%) under RCP8.5 scenario (Table 2b). The GISS-E2-R model shows a greater degree of variation than other models, with a stronger increase in CH_4 burden (+ 153%) and in VOCs emissions (+ 20%) for RCP8.5 (Table 2b).

Excluding CH_4 burden and VOCs emissions, all the RCP scenarios include reductions and redistributions of O_3 precursor emissions throughout the 21st century, due to the air pollution control strategies worldwide. The changes in CH_4 burden are due to the different climate policies in model assumptions. In RCP2.6, CH_4 emissions decrease steadily throughout the century, in RCP4.5 it remain steady until 2050 and then decrease (Voulgarakis et al., 2013) and in RCP8.5 (no climate policy) it rapidly increase compared to 2000. Methane burdens are fixed in the models with no sources, except for the GISS-E2-R simulations in which surface

CH_4 emissions are prescribed for future rather than concentrations (Shindell et al., 2012). The model chemical schemes vary greatly in their complexity, mainly due to the NMVOCs simulations (Young et al., 2013). Isoprene dominates the total NMVOCs emissions (Guenther et al., 1995). In contrast to other models with constant present-day isoprene emissions, the GISS-ES2-R simulations incorporate climate-driven isoprene emissions, with greater BVOC emissions by 2100 and a positive change in total VOCs emissions across RCPs, related to the positive correlation between air temperature and isoprene emission (e.g. Guenther et al., 2006; Arneth et al., 2011; Young et al., 2013).

For RCP2.6 and RCP4.5 scenarios, there is a widespread decrease in O_3 in NH by 2100. The overall decrease in O_3 concentration and AOT40 means for RCP4.5 are about half of that between RCP2.6 and the historical simulation. For both scenarios, the changes are dominated by the decrease in O_3 precursor emissions in the NH extratropics compared to historical simulations (Table 2b). In NOx saturated areas, annual mean O_3 will slightly increase as a result of a less efficient titration by NO, but the overall O_3 burden will decrease substantially at hemispheric scale over time (Gao et al., 2013; Querol et al., 2014; Sicard et al., 2016a). In RCP4.5, Gao et al. (2013) showed that the largest decrease in O_3 (4-10 ppb) occurs in summer at mid-latitudes in the lower troposphere while the O_3 concentrations undergo an increase in winter. During the warm period, the photochemistry plays a major role in the O_3 production, suggesting that the reduction in surface O_3 concentrations is in agreement with the large reduction in anthropogenic O_3 precursor emissions (Sicard et al., 2016a) reducing the extent of regional photochemical O_3 formation (e.g. Derwent et al., 2013; Simpson et al., 2014). Titration effect was also reported by Collette et al. (2012) over Europe by using six chemistry transport models.

The O_3 increase can be also driven by the net impacts of climate change, i.e. increase in stratospheric O_3 intrusion, changing LNOx and impacting reaction rates, through sea surface temperatures and relative humidity changes (Lau et al., 2006; Voulgarakis et al., 2013; Young et al., 2013).

Under the RCP8.5 scenario, the increase in surface O_3 concentrations, by 14% on average, can be attributed to the higher CH_4 emissions coupled with a strong global warming, exceeding 2°C, and a weakened NO titration by reducing NOx emissions (Stevenson et al., 2013; Young et al., 2013). The global CH_4 burden are 27% and 5% lower than 2000, for the RCP2.6 and

RCP4.5 scenarios respectively while for RCP8.5, the total CH_4 burden has more than doubled compared to early 2000s and LNOx emissions increased by 33% (Table 2b). In addition, stronger increases are found over the high-elevation Himalayan Plateau reflecting increased exchange with the free troposphere or stratosphere (Lefohn et al., 2012; Schnell et al., 2016). Several studies reported an increase in the stratospheric O_3 influx and higher stratospheric O_3 levels in response to a warming climate (e.g. Hegglin and Shepherd, 2009; Zeng et al., 2010). The downwards O_3 transport from the stratosphere is an important source of tropospheric O_3 (Hsu and Prather, 2009; Tang et al., 2011), therefore, stratospheric O_3 recovery also plays a partial role (e.g. + 11% for RCP8.5) in surface O_3 burden pattern. As an example, in MOCAGE, smaller reduction in global O_3 mean concentrations (-13%) and higher increase in stratospheric O_3 inputs (+20%) are observed for RCP2.6 (Table 3b). Similarly, for RCP8.5, the highest increase in O_3 mean concentrations (+23%) and stratospheric O_3 (+24%) are recorded in MOCAGE. In addition, lightning NOx emissions show significant upward trend from 2000 to 2100, in particular for the strongest warming scenario (RPC8.5) with greater convective and lightning activity (e.g. Williams, 2009; Lamarque et al., 2013). For RCP8.5, a reduction in surface O_3 concentrations is also simulated over the equatorial region, where the increased relative humidity, in a warmer climate, increases the O_3 loss rate (e.g. Johnson et al., 1999; Zeng and Pyle, 2003).

For RCP2.6 and RCP4.5, absolute decreases are observed for the Mediterranean basin and the Western U.S. due to less precursor emissions in the NH extratropics (e.g. reduction of 5-7 ppb over Europe). Smaller reduction in surface O_3 levels in South and East Asia highlight the smaller changes in O_3 precursor emissions due to the recent emission growth in this region (e.g. Zhang et al., 2009; Xing et al., 2015). For RCP 8.5, the high O_3 increase (up to 10 ppb) in South Asia can be attributed to substantial increase in CH_4 emissions coupled with a strong global warming, exceeding 2°C, and a weakened NO titration and a greater stratospheric O_3 influx (Kawase et al., 2011; Wild et al., 2012; Young et al., 2013).

Risk areas for vegetation under RCP scenarios

Figure 3 shows the changes in the potential O_3 impact on photosynthetic carbon assimilation between present and future. It should be noted that a zero percentage of change (i.e. no change) for IO3, is simulated in sparsely vegetated regions (e.g. Gobi, Sahara, Near East, Western plateau and Greenland), while the change can be higher than 100% when the historical O_3 concentrations are lower than 40 ppb (i.e. AOT40 = 0 and IO3 = 0) and the O_3

concentrations exceed 40 ppb under RCPs (i.e. AOT40 > 0, IO3 > 0). If the AOT40 during the historical period is 0 then the percentage of change is undefined and we have considered and set these grid points as missing values.

The potential O_3 impact for vegetation strongly decreases in NH for RCP2.6, except in MOCAGE where a slight increase in the risk factor (+ 15 %) is simulated at high latitudes and in South Asia. Conversely, the areas where the risk for vegetation increases (> 60 %) occur over Africa (+ 15% to + 60%) for all models, except in CESM-CAM where no change is observed across Africa. Under RCP4.5 scenario, the strongest increase in potential risk for vegetation (> + 60 %) is simulated by MOCAGE, markedly different from the other models, above the latitude 50°N. For all models, the potential O_3 impact for vegetation increases across Africa, from - 15% to + 60% while slight decreases or no change occur worldwide. Under RCP8.5 scenario, an increase of average O_3 over a significant part of the domain is simulated, therefore the exposure to O_3 pollution and impacts on vegetation will increase worldwide by 2100. An increase of the O_3 impacts on vegetation is simulated in Northern U.S., South America, Asia and Africa while a reduction in particular over Eastern U.S. and Southeastern China, and a slight increase (+ 15%) or decrease (- 15%) over Europe depending on the model, are simulated.

In summary, compared to the historical simulations, the averaged relative changes in the O_3 risk factor for the different RCPs are: - 61% for RCP2.6, - 47% for RCP4.5 and + 70% for RCP8.5 (Table 3d). We thus find a significant reduction in risk for vegetation for both RCP2.6 and RCP4.5 scenarios, except in South Africa and at high-latitudes in MOCAGE simulations, and a strong increase in global risk under RCP8.5. Under RCP2.6 and RCP4.5 scenarios, IO3 slightly increases in Africa and over North America and Asia (> latitude 60°N) in MOCAGE. The risk increases over the few areas where the O_3 concentrations increased between the historical period and 2100. Under both scenarios, the strongest reductions in risk are observed over Amazon, Central Africa and South Asia, i.e. where the O_3 concentrations have strongly declined between historical period and 2100. Under the RCP8.5, the areas where the highest projected O_3 mean concentrations are simulated (e.g. Greenland, deserts) are not associated with an increase in IO3 due to the absence of vegetation. Under RCP8.5, IO3 increases worldwide while a reduction is simulated over Southeast North America, northern Amazon, Central Africa and Southeast Asia, and a slighter reduction or a slight increase is simulated over Western Europe (depending on the model).

The spatial pattern of IO3 is consistent with previous analyses on global environmental changes (climate, land-cover, nitrogen deposition, CO_2 fertilization) impacts on vegetation (Nemani et al., 2003; Zhu et al., 2016), i.e. the highest reduction in risk for vegetation, in particular under RCP8.5, occurs over areas where a strong increase in greening, LAI and NPP is observed due to global changes and where a reduction in surface O_3 mean concentrations is found by 2100 (Fig. 1). The regions with the largest greening trends are in Southeast North America, northern Amazon, Europe, Central Africa and Southeast Asia with an average increase of the observed LAI exceeding 0.25 m^2 m^{-2} per year (Zhu et al., 2016). The CO_2 fertilization effects (70%), nitrogen deposition (9%) and climate change (8%) explain the observed greening trend (Zhu et al., 2016). The changing climate alone produces persistent NPP increases and the regions with the highest increase in NPP, ranging from 1.0-1.5% per year, are in Southeast North America, northern Amazon, Western Europe, Central Africa and South Asia (Nemani et al., 2003). From 1982 to 1999, the highest increases are observed in tropical regions, with more than 1.5% per year over Amazon rainforest which accounts for 42% of the global NPP increase (Nemani et al., 2003). Amazon rainforest is one region where the effects are statistically significant. This is particularly important owing to the role of the Amazon rainforests in the global carbon cycle (Zhu et al., 2016). In these areas, we observed a strong increase in NPP and LAI due to warming climate while a reduction in GPP (from - 10 to - 20%) due to O_3 is observed (Sitch et al., 2007). Inversely, the risk for vegetation IO3 increases in particular in Africa, e.g. western Africa along the Gulf of Guinea, in South Brazil and over high-latitudes regions (> 60°N) in North America and Asia where a reduction or a slight increase in LAI (from - 0.05 to + 0.03 m^2 m^{-2} per year) and strong decreases in NPP (1.0-1.5% per year) are simulated (Nemani et al., 2003; Zhu et al., 2016).

Sitch et al. (2007) reported a high GPP reduction due to O_3 effects, between 1901 and 2100 under the *Special Report on Emissions Scenarios A2 emissions* scenario, exceeding 30% in summer over Western Europe, Eastern North America, Amazon, central Africa and South Asia. Previous studies reported that the reductions in GPP simulated by Sitch et al. (2007) are overestimated up to six times due to i) the lack of empirical data about the response of different species to O_3, Sitch et al. (2007) focused on broad-leaved tree, needle-leaved tree, C3 crops, C4 crops and shrubs; ii) the fact that a few experiments have shown no response, e.g. grasslands (Bassin et al., 2013) and iii) the non-inclusion of the nitrogen limitation of growth (Ren et al., 2011; Zak et al., 2011; Kvaleveg and Myhre 2013). In addition, the simulated O_3

concentrations over Amazon forest exceed 90 ppb in summer in Sitch et al. (2007) while the annual O_3 mean is around 15-20 ppb by 2100 in our study.

The projected land covers widely vary under RCPs (Betts et al., 2015). In RCP2.6 scenario, the ground surface covered by croplands increases as a result of bio-energy production, with a more-or-less constant use of grassland. The RCP4.5 scenario focuses on global reforestation programs as part of global climate policy, as a result, the use of cropland and grassland decreases. Under RCP8.5, an increase in croplands and grasslands is applied mostly driven by an increasing global population (van Vuuren et al., 2011). About 50% of forests, grasslands and croplands might be exposed to high O_3 levels by the end of the 21st century (Sitch et al., 2007; Wittig et al., 2009).

Generally, deciduous broadleaf are highly O_3-sensitive risk areas and needleleaf forests are moderately O_3-sensitive risk areas. Crops and grasslands are more sensitive to O_3 exposure than trees and deciduous trees are more sensitive than coniferous trees with lower stomatal conductance (Felzer et al., 2004; Ren et al., 2007; Wittig et al., 2009; Anav et al., 2011). Based on a comparison between Figure 2 and the Global Land Cover Facility maps, we can observe that generally the AOT40, i.e. the potential O_3 risk to vegetation is high over shrublands (e.g. high-latitude region), broadleaf forests (e.g. central Africa), needleleaf forests (e.g. North America) and crops (e.g. South Asia). Under RCP2.6 and RCP4.5, the risk decreases over areas covered by shrublands, savannas and slightly decreases over areas with needleleaf forests in Northern America and Northern Asia. The risk strongly increases over broadleaf forest in Africa and the risk slightly decreases or slightly increases over grasslands (Central Asia and central Africa and U.S.). Under RCP8.5, the largest decreases in risks occur in Eastern U.S., Europe and South-eastern China, where the ground is mainly dominated by croplands, in all models except CESM-CAM.

Conclusions

From six global atmospheric chemistry transport models, we illustrate the changes, i.e. differences for late 21st century relative to the historical run, in ground-level O_3 concentrations and vegetation impact metric (AOT40). Finally, the potential O_3 impacts on photosynthetic carbon assimilation worldwide are investigated to define potential risk areas

for vegetation at global scale by 2100. A major advantage of this study is a comparison between models and scenarios to explore future potential O_3 impacts.

The six models are able to well reproduce the spatial pattern of historical O_3 concentration and AOT40 at global scale, in particular GISS-E2-R and MOCAGE are able to simulate the higher O_3 levels in areas downwind of precursor sources and at the high-elevation areas. The model outputs emphasize the strong asymmetry in the tropospheric O_3 distribution between NH and SH~~; substantially higher O_3 mean concentrations are observed in the NH (ca. 38 ppb), particularly in the latitude band 15-45°N, than in the SH (ca. 23 ppb)~~. The natural emissions of O_3 precursors (e.g. lightning NOx, CO from oceans, isoprene) as well as the complexity of chemical schemes are significant sources of model-to-model differences.

~~In this study, the projected mean surface O_3 concentrations and AOT40 dependent on global and regional emission pathways.~~ Compared to early 2000s, the results suggest changes in surface O_3 of - 9.5 ± 2.0 ppb (NH) and - 1.8 ± 2.1 ppb (SH) in the cleaner RCP2.6 scenario and of + 4.4 ± 2.8 ppb (NH) and + 5.1 ± 2.1 ppb (SH) in RCP8.5 scenario. For RCP2.6 and RCP4.5, absolute decreases are observed for the Mediterranean basin and the Western U.S. due to less precursor emissions in the NH extratropics. ~~(e.g. reduction of 5-7 ppb over Europe). Smaller reduction in surface O_3 levels in South and East Asia highlight the smaller changes in O_3 precursor emissions due to the recent emission growth in this region (e.g. Zhang et al., 2009; Xing et al., 2015).~~ For RCP8.5, all models show climate-driven increases in ground-level O_3 in particular over the Western U.S, Greenland, South Asia and Northeast China and ~~. T~~the changes ranged from + 1-5 ppb ~~in surface O_3~~ over North America and Europe ~~ranged from + 1-5 ppb under RCP8.5~~. ~~South Asia sees the greatest increase, up to more than 10 ppb for RCP 8.5.~~ This O_3 increase can be mainly attributed to substantial increase in CH_4 emissions coupled with a ~~strong~~ global warming~~, exceeding 2°C,~~ and a weakened NO titration ~~and a greater stratospheric O_3 influx (Kawase et al., 2011; Wild et al., 2012; Young et al., 2013). A decline in CH_4 emissions will undoubtedly benefit future O_3 control.~~

Most important results from the study are the spatial patterns and projected changes in global AOT40 and risk areas for vegetation under the RCP scenarios. Even if AOT40 was computed year-round, the global models suggest that despite an improvement under RCP2.6 and RCP4.5, the AOT40-based critical levels for the protection of forests and crops will be

exceeded over many areas of the NH and they may be much more exceeded under RCP8.5 up to a factor exceeding 10 by 2100.

~~Even if AOT40 was computed year-round, the global models suggest that AOT40-based critical levels for the protection of forests and crops will be exceeded over many areas of the NH, and in parts of North America, East and South Asia, and they may be exceeded by a factor exceeding 10 under RCP8.5. AOT40 was used widely during the last two decades, not only in Europe but also in South America (Moura et al., 2014) and Asia (Hoshika et al., 2011) when environmental factors are not limiting, e.g. water availability, air temperature, solar radiation affecting stomata opening (Anav et al., 2016; De Marco et al., 2016).~~

~~As a result, the flux-based metric is introduced as new standard for vegetation protection against effects of O_3, taking into account the modifying effects of multiple climatic and phenological factors on O_3 uptake (Paoletti and Manning, 2007; Sicard et al., 2016b,c).~~

Ozone may be a major threat to biodiversity over large regions of the world ~~(Sicard et al., 2016b)~~, however the size of these areas remains uncertain. The potential O_3 impact on carbon assimilation, IO3, provides a clear indicator of the potential risk to vegetation. By 2100, the potential O_3 impact on photosynthetic carbon assimilation decreases by 61% and 47% under RCP2.6 and RCP4.5, respectively and increases by 70% under RCP8.5, compared to early 2000s over the whole domain. ~~The potential risk areas for vegetation vary worldwide according to the dominant vegetation cover~~. The strongest increase of the O_3 impacts on vegetation is simulated in Northern America and Asia and central Africa. The highest reduction in risk for vegetation (i.e. Southeast North America, the northern Amazon, Central Africa and Southeast Asia) occurs over areas where a strong increase in greening, LAI and NPP is observed and where a reduction in O_3 mean concentrations is found by 2100. ~~enerally, deciduous broadleaf are highly O_3-sensitive risk areas, grasslands and needleleaf forests are moderately O_3-sensitive risk areas. Crops are more sensitive to O_3 exposure than trees and deciduous trees are more sensitive than coniferous trees with lower stomatal conductance (Felzer et al., 2004; Ren et al., 2007; Wittig et al., 2009; Anav et al., 2011).~~

Many ecosystems worldwide are unprotected from O_3 due to the lack of international efforts (Emberson et al., 2014). An efficient reduction in overall O_3 levels is expected over North America and Europe in all RCP scenarios and worldwide if CH_4 emissions are reduced (e.g. Kirtman et al., 2013; Pfister et al., 2014; Schnell et al., 2016). To efficiently protect vegetation against O_3 pollution, suitable standards ~~taking into account the detoxification processes (e.g.~~

~~flux-based metric)~~ are urgently needed and the mitigation actions must be as part of international emission reduction programmes. The flux-based metric is introduced as new standard for vegetation protection against effects of O_3, taking into account the detoxification processes and the modifying effects of multiple climatic and phenological factors on O_3 uptake (Paoletti and Manning, 2007; Sicard et al., 2016b,c). Plant phenology plays a pivotal role in the climate system as it regulates the gas exchange between the biosphere and the atmosphere. Currently, in many O_3 risk assessment studies, the phenology function is based on a simple latitude and topography model and the chemistry models do not take into account the shifts in plant phenology and in start and end date of the growing season; however a first attempt to study the role of phenology on stomatal ozone uptake is shown by Anav et al (2017).

Acknowledgements

This work was carried out with the contribution of the LIFE financial instrument of the European Union (LIFE15 ENV/IT/183) in the framework of the MOTTLES project "Monitoring ozone injury for setting new critical levels" and published within the International Union of Forest Research Organizations (IUFRO) Task Force on Climate Change and Forest Health and IUFRO RG 7.01.09 "Ground-level ozone".

Bibliographic references

Ainsworth E.A., Yendrek C.R., Sitch S., Collins, W.J., Emberson -L.D., 2012, "The effect of Tropospheric Ozone on Net Primary Productivity and Implications for Climate Change". Annu. Rev. Plant Biol. 63: 637-661

Anav A., Liu Q., De Marco A., Proietti C., Savi F., Paoletti E., Piao S., 2017, "The role of plant phenology in stomatal ozone flux modelling". Global Change Biol. doi: 10.1111/gcb.13823

Anav A., Menut L., Khvorostyanov D., Viovy N., 2011, "Impact of tropospheric ozone on the Euro-Mediterranean vegetation". Global Change Biol. 17: 2342-2359

Arbaugh M.J., and Bytnerowicz A., 2003, "Ambient ozone patterns and effects over the Sierra Nevada: synthesis and implications for future research". In: A. Bytnerowicz, M. Arbaugh, R. Alonso (eds), Ozone Air Pollution in the Sierra Nevada: Distribution and Effects on Forests, Developments in Environmental Science, vol. 2, Elsevier, Amsterdam, 249-261

Arneth A., Schurgers G., Lathière J., Duhl T., Beerling D. J., et al., 2011, "Global terrestrial isoprene emission models: sensitivity to variability in climate and vegetation". Atmos. Chem. Phys. 11: 8037-8052

Arneth A., Schurgers G., Hickler T., Miller P.A., 2008, "Effects of species composition, land surface cover, CO_2 concentration and climate on isoprene emissions from European forests". Plant Biol. 10: 150-162

Ashmore M.R., 2005, "Assessing the future global impacts of ozone on vegetation". Plant Cell Environ. 28: 949-964

Ashworth K., Wild O., Hewitt C.N., 2013, "Impacts of biofuel cultivation on mortality and crop yields". Nat. Clim. Change 3: 492-496

Bassin S., Volk M., Fuhrer J., 2013, "Species composition of subalpine grassland is sensitive to nitrogen deposition, but not ozone, after seven years of treatment". Ecosystems 16: 1105-1117

Betts R.A., Golding N., Gonzalez P., Gornall J., Kahana R., et al., 2015, "Climate and land use change impacts on global terrestrial ecosystems and river flows in the HadGEM2-ES Earth system model using the representative concentration pathways". Biogeosciences 12: 1317-1338

Bian J., Yan R., Chen H., Lü D., Massie S.T., 2011, "Formation of the summertime ozone valley over the Tibetan Plateau: The Asian summer monsoon and air column variations". Adv. Atmos. Sci. 28: 1318-1325

Bowman K.W., Shindell D.T., Worden H.M., Lamarque J.F., Young P.J., 2013, "Evaluation of ACCMIP outgoing longwave radiation from tropospheric ozone using TES satellite observations". Atmos. Chem. Phys. 13: 4057-4072

Clifton O.E., Fiore A.M., Correa G., Horowitz L.W., Naik V., 2014, "Twenty-first century reversal of the surface ozone seasonal cycle over the northeastern United States". Geophys. Res. Lett. 41: 7343-7350

Chen X.L., Ma Y.M., Kelder H., Su Z., Yang K., 2011, "On the behaviour of the tropopause folding events over the Tibetan Plateau". Atmos. Chem. Phys. 11: 5113-5122

Chevalier A., Gheusi F., Delmas R., Ordóňez C., Sarrat C., et al., 2007, "Influence of altitude on ozone levels and variability in the lower troposphere: a ground-based study for Western Europe over the period 2001-2004". Atmos. Chem. Phys. 7: 4311-4326

Colette A., Granier C., Hodnebrog Ø., Jakobs H., Maurizi A., et al., 2012, "Future air quality in Europe: a multi-model assessment of projected exposure to ozone". Atmos. Chem. Phys. 12: 10613-10630

Cooper O.R., Parrish D.D., Ziemke J., Balashov N.V., Cupeiro M., 2014, "Global distribution and trends of tropospheric ozone: An observation-based review". Elementa: Science of the Anthropocene 2: 000029

Cooper O.R., Sweeney C., Gao R.S., Tarasick D., Leblanc T., 2012, "Long-term ozone trends at rural ozone monitoring sites across the United States, 1990-2010". J. Geophys. Res. 117: D22307

Cubasch U., Wuebbles D., Chen D., Facchini M.C., Frame D., et al., 2013, "Introduction, in Climate Change 2013: The Physical Science Basis". Contribution of Working Group I to the Fifth Assessment Report of the Intergovernmental Panel on Climate Change, edited by T. F. Stocker et al., Cambridge Univ. Press, Cambridge, U. K. and New York

De Marco A., Sicard P., Vitale M., Carriero G., Renou C., et al., 2015, "Metrics of ozone risk assessment for Southern European forests: canopy moisture content as a potential plant response indicator". Atmos. Environ. 120: 182-190

Derwent R.G., Utembe S.R., Jenkin M.E., Shallcross D.E., 2015, "Tropospheric ozone production regions and the intercontinental origins of surface ozone over Europe".Atmos. Environ. 112: 216-224

Derwent R.G., Manning A.J., Simmonds P.G., Spain T.G., O'Doherty S., 2013, "Analysis and interpretation of 25 years of ozone observations at the Mace Head Atmospheric Research Station on the Atlantic Ocean coast of Ireland from 1987 to 2012". Atmos. Environ. 80: 361-368

Derwent R.G., Witham C.S., Utembe S.R., Jenkin M.E., Passant N.R., 2010, "Ozone in Central England: the impact of 20 years of precursor emission controls in Europe". Environ. Sci. Policy 13: 195-204

Donner L.J., Wyman B.L., Hemler R.S., Horowitz L.W., Ming Y., et al., 2011, "The dynamical core, physical parameterizations, and basic simulation characteristics of the atmospheric component AM3 of the GFDL Global Coupled Model CM3". J. Climate 24: 3484-3519

European Environment Agency, 2015 "Air quality in Europe - 2015 report".ISBN 978-92-9213-702-1. Report No 5/2015

Ellingsen K., Gauss M., Van Dingenen R., Dentener F.J., Emberson L., et al., 2008, "Global ozone and air quality: a multi-model assessment of risks to human health and crops". Atmos. Chem. Phys. 8: 2163-2223

Emberson L.D., Fuhrer J., Ainsworth L., Ashmore M.R., 2014, "Biodiversity and Ground-level Ozone". Report UNEP/CBD/SBSTTA/18/INF/17. Convention on Biological Diversity, 18th meeting, Montreal, 23-28 June 2014

Fares S., Vargas R., Detto M., Goldstein A.H., Karlik J., et al., 2013, "Tropospheric ozone reduces carbon assimilation in trees: estimates from analysis of continuous flux measurements". Global Change Biol.19: 2427-2443

Federal Register, 2015, "National Ambient Air Quality Standards for Ozone". 40 CFR Part 50, 51, 52, 53, and 58, pp 65292-65468

Felzer B.S.F., Kicklighter D.W., Melillo J.M., Wang C., Zhuan Q., et al., 2004, "Ozone effects on net primary production and carbon sequestration in the conterminous United States using a biogeochemistry model". Tellus B 56: 230-248

Fiore A.M., Naik V., Leibensperger E.M., 2015, "Air quality and climate connections". J. Air Waste Manage. Assoc. 65: 645-685

Fiore A.M., Naik V.,Spracklen D.V., Steiner A., Unger N. et al., 2012, "Global air quality and climate". Chem. Soc. Rev. 41: 6663-6683

Fiscus E.L., Booker F.L., Burkey K.O., 2005, "Crop responses to ozone: uptake, modes of action, carbon assimilation and partitioning". Plant Cell Environ. 28: 997-1011

Gao Y., Fu J.S., Drake J.B., Lamarque J.F., Liu Y., 2013, "The impact of emission and climate change on ozone in the United States under representative concentration pathways (RCPs)". Atmos. Chem. Phys. 13: 9607-9621

Granier C., Niemeier U., Jungclaus J.H., Emmons L., Hess P., et al., 2006, "Ozone pollution from future ship traffic in the Arctic northern passages". Geophys. Res. Lett. 33, doi: 10.1029/2006GL026180

Guenther A.B., Karl T., Harley P., Wiedinmyer C., Palmer P.I., Geron C., 2006, "Estimates of global terrestrial isoprene emissions using MEGAN (Model of Emissions of Gases and Aerosols from Nature)". Atmos. Chem. Phys. 6: 3181-3210

Guenther A.B., Hewitt C.N., Erickson D., Fall R., Geron, C., et al., 1995, "A global model of natural volatile organic compound emissions". J. Geophys. Res. 100: 8873-8892

Guo D., Su Y., Shi C., Xunn J., Powell Jr. A.M., 2015, "Double core of ozone valley over the Tibetan Plateau and its possible mechanisms". Journal of Atmospheric and Solar-Terrestrial Physics 130: 127-131

Hegglin M.I. and Shepherd T.G., 2009, "Large climate-induced changes in ultraviolet index and stratosphere-to-troposphere ozone flux". Nature Geosci. 2: 687

Helmig D., Oltmans S.J., Morse T.O., Dibb J.E., 2007, "What is causing high ozone at Summit, Greenland?". Atmos. Environ. 41: 5031-5043

Hess P.G. and Zbinden R., 2013, "Stratospheric impact on tropospheric ozone variability and trends: 1990-2009". Atmos. Chem. Phys. 13: 649-674

Holland M., Kinghorn S., Emberson L., Cinderby S., Ashmore M., et al., 2006, "Development of a framework for probabilistic assessment of the economic losses caused by ozone damage to crops in Europe". UNECE International Cooperative Programme on Vegetation. Contract Report EPG 1/3/205. CEH Project No: C02309NEW

Hoshika Y., Shimizu Y., Omasa K., 2011, "A comparison between stomatal ozone uptake and AOT40 of deciduous trees in Japan". iForest – Biogeosciences and Forestry doi: 10.3832/ifor0573-004

Hsu J. and Prather M.J., 2009, "Stratospheric variability and tropospheric ozone". J. Geophys. Res. 114: D06102

Hu X.M, Klein Petra M., Xue M. et al., 2013, "Impact of the vertical mixing induced by low-level jets on boundary layer ozone concentration". Atmos. Environ. 70: 123-130

Hudson R.D., Andrade M.F., Follette M.B., Frolov A.D., 2006, "The total ozone field separated into meteorological regimes – Part II: Northern Hemisphere mid-latitude total ozone trends". Atmos. Chem. Phys. 6: 5183-5191

IPCC, Intergovernmental Panel on Climate Change, 2014, "Summary for Policymakers". In: "Climate Change 2014: Impacts, Adaptation and Vulnerability". Contribution of Working Group II to the Fifth Assessment Report of the Intergovernmental Panel on Climate Change. Cambridge University Press, Cambridge, UK

Jeričević A., Koračin D., Jiang J., Chow J., Watson J., et al., 2013, "Air Quality Study of High Ozone Levels in South California". Part of the series NATO Science for Peace and Security Series C: Environmental Security. Air Pollution Modeling and its Application XXII: 629-633

Johnson C.E., Collins W.J., Stevenson D.S., Derwent R.G., 1999, "Relative roles of climate and emissions changes on future tropospheric oxidant concentrations". J. Geophys. Res. 104: 18631-18645

Josse B., Simon P., Peuch V.H., 2004, "Radon global simulations with the multiscale chemistry and transport model MOCAGE". Tellus-B 56: 339-356

Kawase H., Nagashima T., Sudo K., Nozawa T., 2011, "Future changes in tropospheric ozone under Representative Concentration Pathways (RCPs)". Geophys. Res. Lett. 38: L05801

Kelly J., Makar P.A., Plummer D.A., 2012, "Projections of mid-century summer air-quality for North America: effects of changes in climate and precursor emissions". Atmos. Chem. Phys. 12: 5367-5390

Kirtman B., Power S.B., Adedoyin J.A., Boer G.J., Bojariu R., et al., 2013, "Near-term climate change: Projections and predictability, in Climate Change 2013: The Physical Science Basis". Contribution of Working Group I to the Fifth Assessment Report of the Intergovernmental Panel on Climate Change, edited by T.F. Stocker et al., Cambridge Univ. Press, Cambridge, U. K., and New York

Klingberg J., Engardt M., Karlsson P.E., Langner J., Pleijel H., 2014, "Declining ozone exposure of European vegetation under climate change and reduced precursor emissions". Biogeosciences 11: 5269-5283

Krinner G., Viovy N., de Noblet-Ducoudré N., Ogée J., Polcher J., et al., 2005, "A dynamic global vegetation model for studies of the coupled atmosphere-biosphere system". Global Biogeochem. Cy. 19: GB1015

Kulkarni P.S., Bortoli D., Domingues A., Silva A.M., 2015, "Surface Ozone Variability and Trend over Urban and Suburban Sites in Portugal". Aerosol Air Qual. Res.: 1-15

Kulkarni P.S., Bortoli D., Salgado R., Anton M., Costa M.J., et al., 2011, "Tropospheric ozone variability over the Iberian Peninsula". Atmos. Environ. 45: 174-182

Kvalevag M.M. and Myrhe G., 2013, "The effect of carbon-nitrogen coupling on the reduced land carbon sink caused by ozone". Geophys. Res. Lett. 40: 3227-3231

Lamarque J.F., Shindell D.T., Josse B., Young P.J., Cionni I., et al., 2013, "The Atmospheric Chemistry and Climate Model Intercomparison Project (ACCMIP): overview and description of models, simulations and climate diagnostics". Geosci. Model Dev. 6: 179-206

Lamarque J.F., Emmons L.K., Hess P.G., Kinnison D.E., Tilmes, S., et al., 2012, "CAM-chem: description and evaluation of interactive atmospheric chemistry in the Community Earth System Model". Geosci. Model Dev. 5: 369-411

Lamarque J.F., Bond T.C., Eyring V., Granier C., Heil A., et al., 2010, "Historical (1850–2000) gridded anthropogenic and biomass burning emissions of reactive gases and aerosols: methodology and application". Atmos. Chem. Phys. 10: 7017-7039

Lamarque J.F., Hess P.G., Emmons L.K., Buja L.E., Washington W.M., Granier C., 2005, "Tropospheric ozone evolution between 1890 and 1990". J. Geophys. Res. 110: D08304

Langner J., Engardt M., Baklanov A., Christensen J.H., Gauss M., et al., 2012, "A multi-model study of impacts of climate change on surface ozone in Europe". Atmos. Chem. Phys. 12: 10423-10440

Lau N.C., Leetmaa A., Nath M.J., 2006, "Attribution of atmospheric variations in the 1997-2003 period to SST anomalies in the Pacific and Indian Ocean basins". J. Climate 19: 3607-3628

Lee Y.H.and Adams P.J., 2011, "A fast and efficient version of the two-moment aerosol sectional (TOMAS) global aerosol microphysics model". Aerosol Sci. Tech. 46: 678-689

Lefohn A.S., Malley C.S., Simon H., Wells B., Xu X., et al., 2017, "Responses of human health and vegetation exposure metrics to changes in ozone concentration distributions in the European Union, United States, and China". Atmos. Environ. 152: 123-145

Lefohn A.S., Emery C., Shadwick D., Wernli H., Jung J., OltmansS.J.,2014, "Estimates of background surface ozone concentrations in the United States based on model-derived source apportionment". Atmos. Environ. 84:275-288.

Lefohn A.S., Wernli H., Shadwick D., Oltmans S.J., Shapiro M., 2012, "Quantifying the frequency of stratospheric-tropospheric transport affecting enhanced surface ozone concentrations at high- and low-elevation monitoring sites in the United States". Atmos. Environ. 62: 646-656

Lefohn A.S., Shadwick D., Oltmans S.J., 2010, "Characterizing changes in surface ozone levels in metropolitan and rural areas in the United States for 1980-2008 and 1994-2008". Atmos. Environ. 44: 5199-5210

Legrand M.,Preunkert S., Jourdain B., Gallée H., Goutail F., et al., 2009, "Year-round record of surface ozone at coastal (Dumont d'Urville) and inland (Concordia) sites in East Antarctica". J. Geophys. Res. 114: doi: 10.1029/2008JD011667

Liu C., Liu Y., Cai Z., Gao S., Bian J., et al., 2010, "Dynamic formation of extreme ozone minimum events over the Tibetan Plateau during northern winters 1987-2001". J. Geophys. Res. 115: D18311

Meinshausen M., Wigley T.M.L., Raper S.C.B., 2011, "Emulating atmosphere-ocean and carbon cycle models with a simpler model, MAGICC6 - Part 2: Applications". Atmos. Chem. Phys. 11: 1457-1471

Mills G., Hayes F., Simpson D., Emberson L., Norris D., et al., 2011, "Evidence of widespread effects of ozone on crops and (semi-)natural vegetation in Europe (1990-2006) in relation to AOT40 and flux-based risk maps". Global Change Biol. 17: 592-613

Monks P.S., Archibald A.T., Colette A., Cooper O., Coyle M., et al., 2015, "Tropospheric ozone and its precursors from the urban to the global scale from air quality to short-lived climate forcer". Atmos. Chem. Phys. 15: 8889-8973

Moura B.B., Alves E.S., de Souza S.R., Domingos M., Vollenweider P., 2014, "Ozone phytotoxic potential with regard to fragments of the Atlantic Semi-deciduous Forest downwind of Sao Paulo, Brazil". Environ. Pollut. 192: 65-73

Myhre G., Shindell D., Bréon F.M., Collins W., Fuglestvedt J., et al., 2013, "Anthropogenic and Natural Radiative Forcing". In: Climate Change 2013: The Physical Science Basis. Contribution of Working Group I to the Fifth Assessment Report of the Intergovernmental Panel on Climate Change. Cambridge University Press, Cambridge, United Kingdom and New York, USA

Naik V., Voulgarakis A., Fiore A.M., Horowitz L.W., Lamarque J.F., et al., 2012, "Preindustrial to present day changes in tropospheric hydroxyl radical and methane lifetime from the Atmospheric Chemistry and Climate Model Intercomparison Project (ACCMIP)". Atmos. Chem. Phys. Discuss. 12: 30755-30804

Nazarenko L., Schmidt G.A., Miller R.L., Tausnev N., Kelley M., et al., 2015, "Future climate change under RCP emission scenarios with GISS ModelE2". J. Adv. Model. Earth Syst. 7: 244-267

Nemani R.R., Keeling C.D., Hashimoto H., Jolly W.M., Piper S.C., et al., 2003, "Climate-Driven Increases in Global Terrestrial Net Primary Production from 1982 to 1999".Science 300: 1560-1563

Ollinger S.V., Aber J.D., Reich P.B., 1997, "Simulating ozone effects on forest productivity: interactions among leaf, canopy, and stand-level processes". Ecol. Appl. 7: 1237-1251.

Oltmans S.J., Lefohn A.S., Harris J.M., Galbally I., Scheel H.E., et al., 2006, "Long-term changes in tropospheric ozone". Atmos. Environ. 40: 3156-3173

Paoletti E., De Marco A., Beddows D.C.S., Harrison R.M., Manning W.J., 2014, "Ozone levels in European and USA cities are increasing more than at rural sites, while peak values are decreasing". Environ. Pollut. 192: 295-299

Paoletti E. and Manning W.J., 2007, "Toward a biologically significant and usable standard for ozone that will also protect plants". Environ. Pollut. 150: 85-95

Paoletti E., 2006, "Impact of ozone on Mediterranean forest: A review". Environ. Pollut. 144: 463-474

Parrish D.D., Law K.S., Staehelin J., Derwent R., Cooper O.R., et al., 2012, "Long-term changes in lower tropospheric baseline ozone concentrations at northern mid-latitudes". Atmos. Chem. Phys. 12: 11485-11504

Pfister G.G., Walters S., Lamarque J.F., Fast J., Barth M.C., et al., 2014, "Projections of future summertime ozone over the U.S". J. Geophys. Res. Atmos. 119: 5559-5582

Price C. and Rind D.H., 1992, "A simple lightning parameterization for calculating global lightning distributions". J. Geophys. Res., 97: 9919-9933
Proietti C., Anav A., De Marco A., Sicard P., Vitale M., 2016, "A multi-sites analysis on the ozone effects on Gross Primary Production of European forests". Sci. Total Environ. 556: 1-11
Querol X., Alastuey A., Pandolfi M., Reche C., Pérez N., et al., 2014, "2001-2012 trends on air quality in Spain". Sci. Total Environ. 490: 957-969.
Reich P.B., 1987, "Quantifying plant response to ozone: a unifying theory". Tree Physiol. 3: 63-91
Ren W., Tian H., Liu M., Zhang C., Chen G., et al., 2007, "Effects of tropospheric ozone pollution on net primary productivity and carbon storage in terrestrial ecosystems of China". J. Geophys. Res. 112: 1-17
Riahi K., Rao S., Krey V., Cho C., Chirkov V., et al., 2011, "RCP 8.5 - A scenario of comparatively high greenhouse gas emissions". Climatic Change 109: 33-57
Rieder H.E., Fiore A.M., Horowitz L.W., Naik V., 2015, "Projecting policy-relevant metrics for high summertime ozone pollution events over the eastern United States due to climate and emission changes during the 21stcentury". J. Geophys. Res. Atmos. 120: 784-800
Ridley B.A., Pickering K.E., Dye, J.E., 2005, "Comments on the parameterization of lightning-produced NO in global chemistry-transport models". Atmos. Environ. 39: 6184-6187
Ochoa-Hueso R., Munzi S., Alonso R., Sicard P., Stevens C. et al., 2017, "Ecological Impacts of Atmospheric Pollution and Interactions with Climate Change in Terrestrial Ecosystems of the Mediterranean Basin: Current Research and Future Directions". Environ. Pollut. 227: 194-206
Sanderson M.G., Collins W.J., Hemming D.L., Betts R.A., 2007, "Stomatal conductance changes due to increasing carbon dioxide levels: Projected impact on surface ozone levels". Tellus 59B: 404-411
Sanderson M.G., Jones C.D., Collins W.J., Johnson C.E., Derwent R.G., 2003, "Effect of climate change on isoprene emissions and surface ozone levels". Geophys. Res. Lett. 30: 1936
Schnell J.L., Prather M.J., Josse B., Naik V., Horowitz L.W., et al., 2016, "Effect of climate change on surface ozone over North America, Europe, and East Asia". Geophys. Res. Lett.43: L068060
Seidel D.J., Fu Q., Randel W.J., Reichler T.J., 2008, "Widening of the tropical belt in a changing climate". Nat. Geosci 1: 21-4
Shindell D.T., Lamarque J.F., Schulz M., Flanner M., Jiao C., et al., 2012, "Radiative forcing in the ACCMIP historical and future climate simulations".Atmos. Chem. Phys. Discuss. 12: 21105-21210
Shindell D.T., Faluvegi G., Stevenson D.S., Krol M.C., Emmons L.K., et al., 2006, "Multi-model simulations of carbon monoxide: Comparison with observations and projected near-future changes". J. Geophys. Res. 111: D19306
Sicard P., Serra R., Rossello P., 2016a, "Spatiotemporal trends of surface ozone concentrations and metrics in France". Environ. Res. 149: 122-144
Sicard P, Augustaitis A., Belyazid S., Calfapietra C., De Marco A., et al., 2016b, "Global topics and novel approaches in the study of air pollution, climate change and forest ecosystems". Environ. Pollut.213: 977-987
Sicard P., De Marco A., Dalstein-Richier L., Tagliaferro F., Paoletti E., 2016c, "An epidemiological assessment of stomatal ozone flux-based critical levels for visible ozone injury in Southern European forests". Sci. Total Environ. 541: 729-741

Sicard P., De Marco A., Troussier F., Renou C., Vas N., Paoletti E., 2013, "Decrease in surface ozone concentrations at Mediterranean remote sites and increase in the cities". Atmos. Environ. 79: 705-715

Sicard P., Vas N., Dalstein-Richier L., 2011, "Annual and seasonal trends for ambient ozone concentration and its Impact on Forest Vegetation in Mercantour National Park (South-eastern France) over the 2000-2008 period". Environ. Pollut. 159: 351-362

Sicard P., Coddeville P., Galloo J.C., 2009, "Near-surface ozone levels and trends at rural stations in France over the 1995-2003 period". Environ. Monit. Assess. 156: 141-157

Simpson D., Arneth A., Mills G., Solberg S., Uddling J., 2014, "Ozone - the persistent menace: interactions with the N cycle and climate change". Curr. Opin. Env. Sust. 9-10: 9-19

Singh H.B., Herlth D., O'Hara D., Zahnle K., Bradshaw J.D., et al., 1992, "Relationship of Peroxyacetyl nitrate to active and total odd nitrogen at northern high latitudes: influence of reservoir species on NOx and O_3". J. Geophys. Res. 97:16523-30

SitchS., Cox P.M., Collins W.J., Huntingford C., 2007, "Indirect radiative forcing of climate change through ozone effects on the land-carbon sink". Nature 448: 791-794

Steinbacher M., Henne S., Dommen J., Wiesen P., Prevot A.S.H., 2004, "Nocturnal trans-alpine transport of ozone and its effects on air quality on the Swiss Plateau". Atmos. Environ. 38: 4539-4550

Stevenson D.S., Young P.J., Naik V., Lamarque J.F., Shindell D.T., et al., 2013, "Tropospheric ozone changes, radiative forcing and attribution to emissions in the Atmospheric Chemistry and Climate Model Inter-comparison Project (ACCMIP)". Atmos. Chem. Phys. 13: 3063-3085

Stevenson D.S., Young P.J., Naik V., Lamarque J.F., Shindell D.T., et al., 2012, "Tropospheric ozone changes, radiative forcing and attribution to emissions in the Atmospheric Chemistry and Climate Model Inter-comparison Project (ACCMIP)". Atmos. Chem. Phys. Discuss. 12: 26047-26097

Stevenson D.S., Dentener F.J., Schultz M.G., Ellingsen K., van Noije T.P.C., et al., 2006, "Multi-model ensemble simulations of present-day and near-future tropospheric ozone". J. Geophys. Res. 111: D08301

Stevenson D.S., Johnson C.E., Collins W.J., Derwent R.G., Edwards J.M., 2000, "Future estimates of tropospheric ozone radiative forcing and methane turnover – The impact of climate change". Geophys. Res. Lett. 27: 2073-2076

Stohl A., Berg T., Burkhart J.F., Fjaeraa A.M., Forster C., et al., 2007, « Arctic smoke - record high air pollution levels in the European Arctic due to agricultural fires in Eastern Europe in spring 2006".Atmos. Chem. Phys. 7: 511-534

Tang Q., Prather M.J., Hsu J., 2011, "Stratosphere-troposphere exchange ozone flux related to deep convection". Geophys. Res. Lett. 38: L03806

Teyssèdre H., Michou M., Clark H.L., Josse B., Karcher F., et al., 2007, "A new tropospheric and stratospheric Chemistry and Transport Model MOCAGE-Climat for multi-year studies: evaluation of the present-day climatology and sensitivity to surface processes". Atmos. Chem. Phys. 7: 5815-5860

Tian W., Chipperfield M., Huang Q., 2008, "Effects of the Tibetan Plateau on total column ozone distribution". Tellus 60B: 622-635

UNECE, United Nations Economic Commission for Europe. Convention on Long-Range Trans-boundary Air Pollution, 2010, "Mapping Critical Levels for Vegetation". nternational Cooperative Programme on Effects of Air Pollution on Natural Vegetation and Crops, Bangor, UK

van Vuuren D., Edmonds J., Kainuma M., Riahi K., Thomson A., et al., 2011, "The representative concentration pathways: an overview". Climatic Change 109: 5-31

Voulgarakis A., Naik V., Lamarque J.F., Shindell D.T., Young P.J. et al., 2013, "Analysis of present day and future OH and methane lifetime in the ACCMIP simulations". Atmos. Chem. Phys. 13: 2563-2587

Walker T.W.,Jones D.B.A., Parrington M., Henze D.K., Murray L.T., et al., 2012, "Impacts of mid-latitude precursor emissions and local photochemistry on ozone abundances in the Arctic". Journal of Geophysical Research: Atmospheres 117, doi: 10.1029/2011JD016370

Wang Q.Y., Gao R.S., Cao J.J., Schwarz J.P., Fahey D.W., et al. 2015, "Observations of high level of ozone at Qinghai Lake basin in the northeastern Qinghai-Tibetan Plateau, western China". J. Atm. Chem. 72: 19-26

Wang X.and Mauzerall D.L., 2004, "Characterizing distributions of surface ozone and its impact on grain production in China, Japan and South Korea: 1900 and 2020". Atmos. Environ. 38: 4383-4402

Watanabe S., Hajima T., Sudo K., Nagashima T., Takemura T., et al., 2011, "MIROC-ESM 2010: model description and basic results of CMIP5-20c3m experiments". Geosci. Model Dev. 4: 845-872

Wesely M.L. and Hicks B.B., 2000, "A review of the current status of knowledge in dry deposition". Atmos. Environ. 34: 2261-2282

Wild O., Fiore A.M., Shindell D.T., Doherty R.M., Collins W.J., et al., 2012, "Modelling future changes in surface ozone: a parameterized approach". Atmos. Chem. Phys. 12: 2037-2054

Wild O., 2007, "Modelling the global tropospheric ozone budget: exploring the variability in current models". Atmos. Chem. Phys. 7: 2643-2660

Williams E.R., 2009, "The global electrical circuit: A review". Atmos. Res., 91: 140-152.

Wilson R.C., Fleming Z. L., Monks P. S., Clain G., Henne S., et al., 2012, "Have primary emission reduction measures reduced ozone across Europe? An analysis of European rural background ozone trends 1996-2005".Atmos. Chem. Phys. 12: 437-454

Wittig V.E., Ainsworth E.A., Naidu S.L., Karnosky D.F., Long S.P., 2009, "Quantifying the impact of current and future tropospheric ozone on tree biomass, growth, physiology and biochemistry: a quantitative meta-analysis". Global Change Biol.15: 396-424

Wittig V.E., Ainsworth E.A., Long S.P., 2007,"To what extent do current and projected increases in surface ozone affect photosynthesis and stomatal conductance of trees? A meta-analytic review of the last 3 decades of experiments". Plant, Cell Environ. 30: 1150-1162

Xing J., Mathur R., Pleim J., C. Hogrefe, Gan C.M., et al., 2015, "Observations and modeling of air quality trends over 1990–2010 across the Northern Hemisphere: China, the United States and Europe". Atmos. Chem. Phys. 15: 2723-2747

Young P.J., Archibald A.T., Bowman K.W., Lamarque J.F., Naik V., et al., 2013, "Preindustrial to end 21st century projections of tropospheric ozone from the Atmospheric Chemistry and Climate Model Intercomparison Project (ACCMIP)". Atmos. Chem. Phys. 13: 2063-2090

Zak D.R., Pregitzer K.S., Kubiske M.E., Burton A.J., 2011, "Forest productivity under elevated CO_2 and O_3; positive feedbacks to soil N cycling sustain decade-long net primary productivity enhancement by CO_2. Ecology Letters 14: 1220-1226

Zeng G., Morgenstern O., Braesicke P., Pyle J.A., 2010, "Impact of stratospheric ozone recovery on tropospheric ozone and its budget". Geophys. Res. Lett. 37: L09805

Zeng G., Pyle J.A., Young P. J., 2008, "Impact of climate change on tropospheric ozone and its global budgets, Atmos. Chem. Phys. 8: 369-387

Zeng G. and Pyle J.A., 2003, "Changes in tropospheric ozone between 2000 and 2100 modeled in a chemistry-climate model". Geophys. Res. Lett. 30: 1392

Zhang Q., Streets D.G., Carmichael G.R., He K.B., Huo H., et al., 2009, "Asian emissions in 2006 for the NASA INTEX-B mission". Atmos. Chem. Phys. 9: 5131-5153

Zhang M.,Xu Y., Uno I., Akimoto H., 2004, "A numerical study of tropospheric ozone in the springtime in east Asia". Adv. Atmos. Sci. 21: 163-170

Zhang L., Brook J. R., Vet R., 2003, "A revised parameterization for gaseous dry deposition in air-quality models". Atmos. Chem. Phys. 3: 2067-2082

Zhu Z., Piao S., Myneni R.B., Huang M., Zeng Z., et al., 2016, "Greening of the Earth and its drivers". Nature Climate Change 6: 791-795

Figure 1: Surface ozone average concentrations (in ppb) at the lower model layer for each ACCMIP model over the historical period and for RCP2.6, RCP4.5 and RCP8.5 simulations by 2100. The data are missing for 2 models under RCP4.5 ("No contour data").

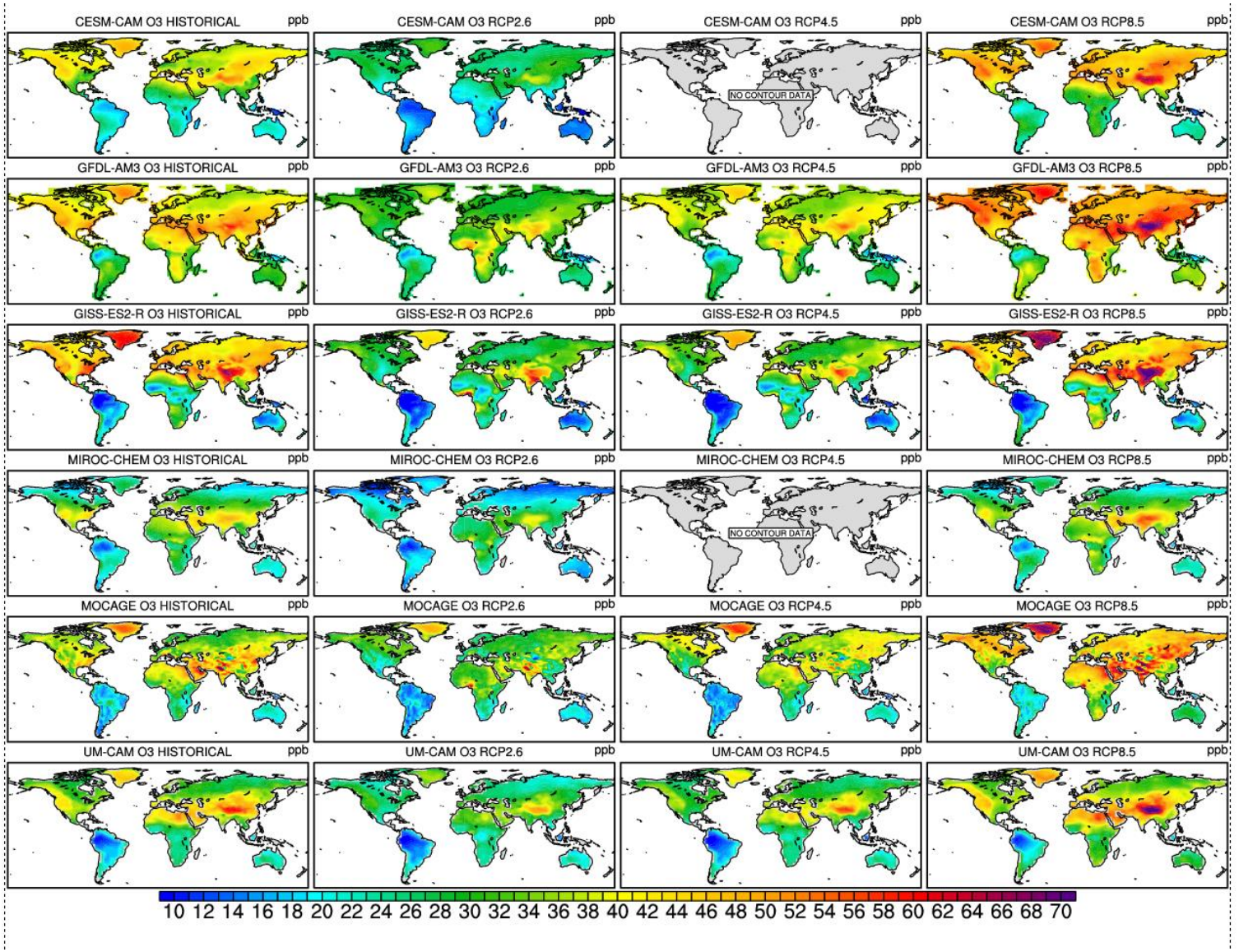
CESM-CAM O3 HISTORICAL ppb
CESM-CAM O3 RCP2.6 ppb
CESM-CAM O3 RCP4.5 ppb
NO CONTOUR DATA
CESM-CAM O3 RCP8.5 ppb
GFDL-AM3 O3 HISTORICAL ppb
GFDL-AM3 O3 RCP2.6 ppb
GFDL-AM3 O3 RCP4.5 ppb
GFDL-AM3 O3 RCP8.5 ppb
GISS-ES2-R O3 HISTORICAL ppb
GISS-ES2-R O3 RCP2.6 ppb
GISS-ES2-R O3 RCP4.5 ppb
GISS-ES2-R O3 RCP8.5 ppb
MIROC-CHEM O3 HISTORICAL ppb
MIROC-CHEM O3 RCP2.6 ppb
MIROC-CHEM O3 RCP4.5 ppb
NO CONTOUR DATA
MIROC-CHEM O3 RCP8.5 ppb
MOCAGE O3 HISTORICAL ppb
MOCAGE O3 RCP2.6 ppb
MOCAGE O3 RCP4.5 ppb
MOCAGE O3 RCP8.5 ppb
UM-CAM O3 HISTORICAL ppb
UM-CAM O3 RCP2.6 ppb
UM-CAM O3 RCP4.5 ppb
UM-CAM O3 RCP8.5 ppb
10 12 14 16 18 20 22 24 26 28 30 32 34 36 38 40 42 44 46 48 50 52 54 56 58 60 62 64 66 68 70

1037
1038

Figure 2: Surface mean AOT40 (in ppm.h) at the lower model layer for each ACCMIP model over the historical period and for RCP2.6, RCP4.5 and RCP8.5 simulations by 2100. The data are missing for 2 models under RCP4.5 ("No contour data").

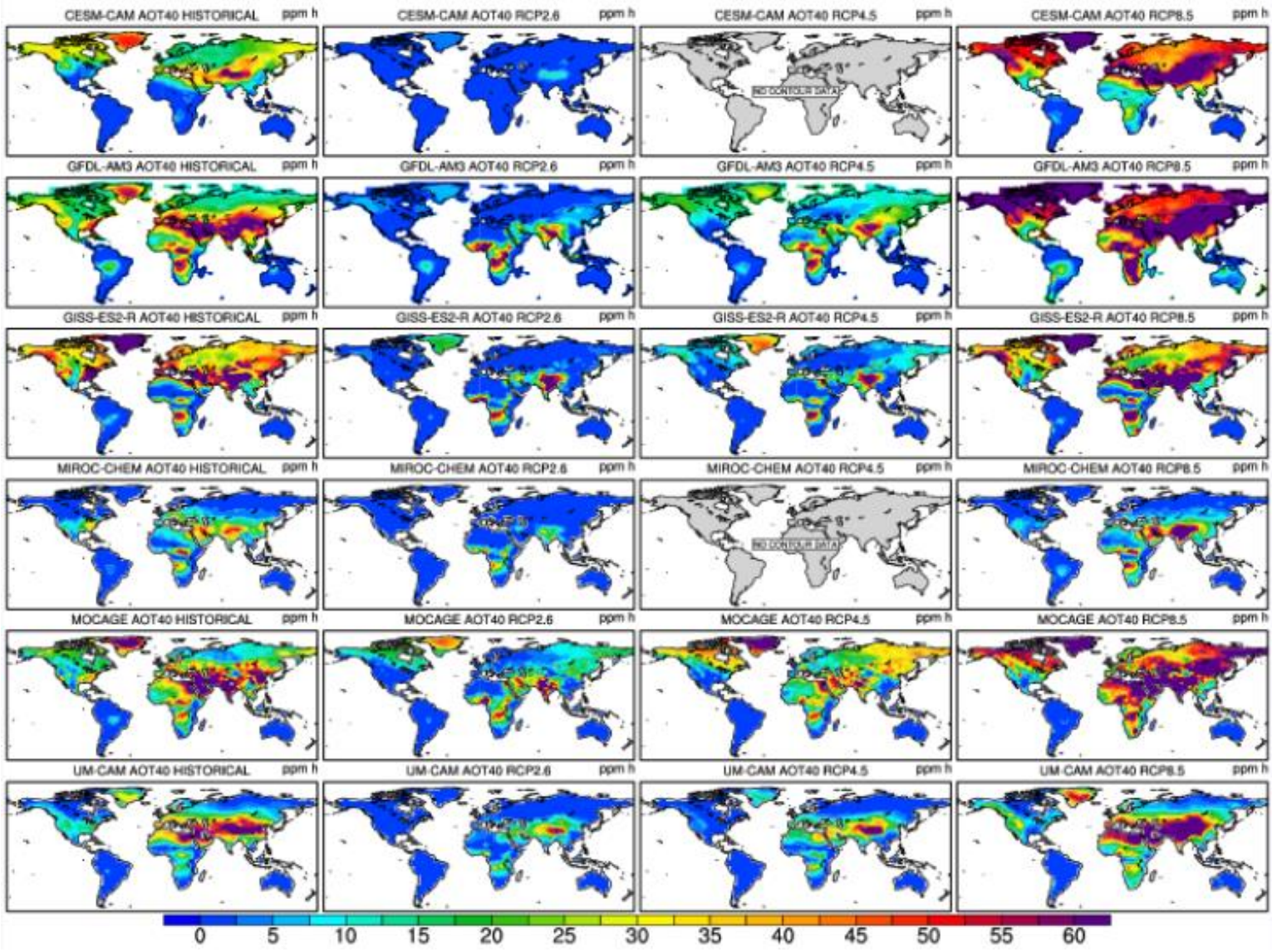

Figure 3: Simulated percentage changes (%) in the potential ozone impact on photosynthetic carbon assimilation (IO3) for each ACCMIP model between RCP2.6, RCP4.5 and RCP8.5 simulations and the historical run. The data are missing for 2 models under RCP4.5 ("No contour data").

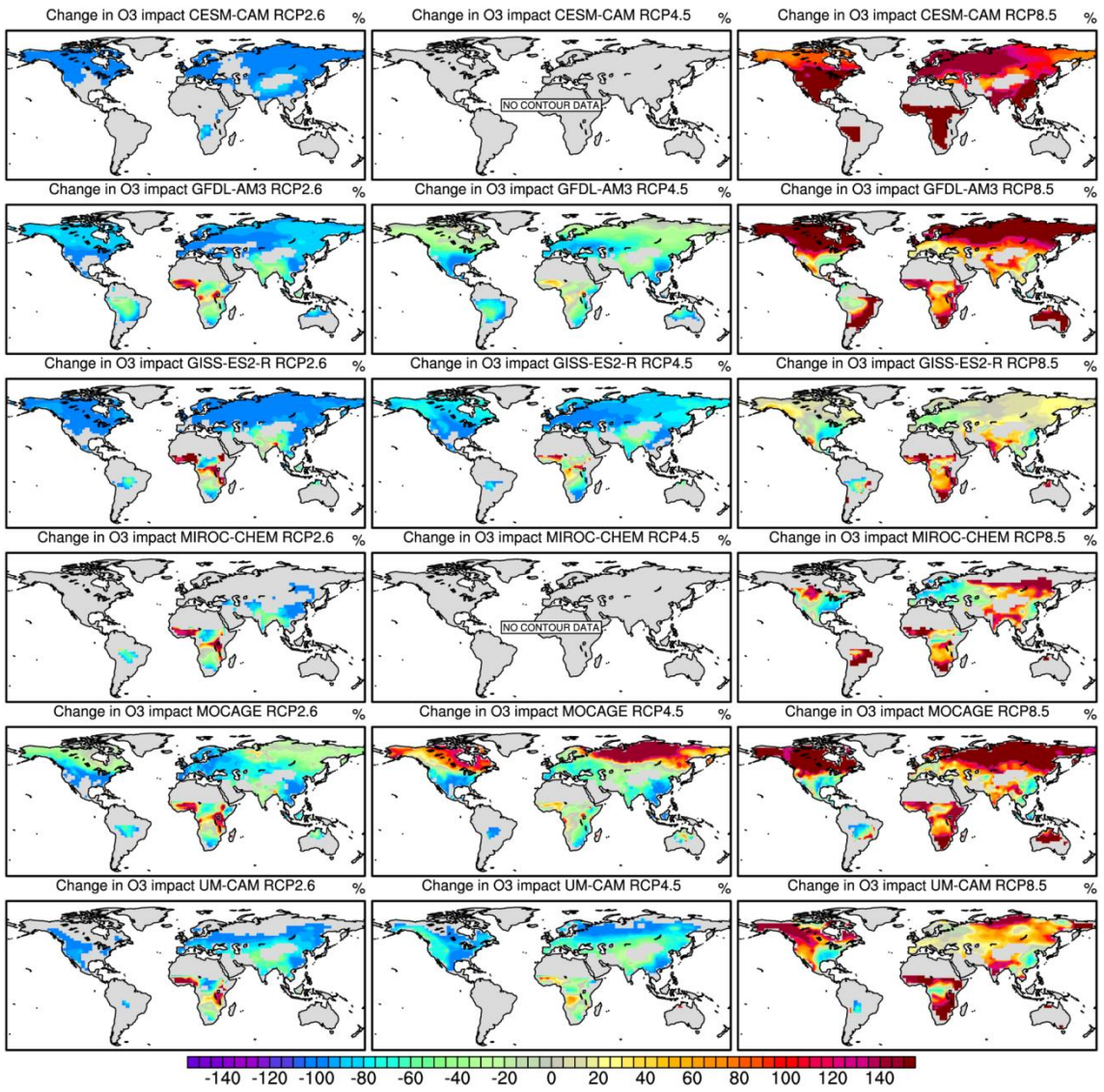
Change in O3 impact CESM-CAM RCP2.6 %
Change in O3 impact CESM-CAM RCP4.5 %
NO CONTOUR DATA
Change in O3 impact CESM-CAM RCP8.5 %
Change in O3 impact GFDL-AM3 RCP2.6 %
Change in O3 impact GFDL-AM3 RCP4.5 %
Change in O3 impact GFDL-AM3 RCP8.5 %
Change in O3 impact GISS-ES2-R RCP2.6 %
Change in O3 impact GISS-ES2-R RCP4.5 %
Change in O3 impact GISS-ES2-R RCP8.5 %
Change in O3 impact MIROC-CHEM RCP2.6 %
Change in O3 impact MIROC-CHEM RCP4.5 %
NO CONTOUR DATA
Change in O3 impact MIROC-CHEM RCP8.5 %
Change in O3 impact MOCAGE RCP2.6 %
Change in O3 impact MOCAGE RCP4.5 %
Change in O3 impact MOCAGE RCP8.5 %
Change in O3 impact UM-CAM RCP2.6 %
Change in O3 impact UM-CAM RCP4.5 %
Change in O3 impact UM-CAM RCP8.5 %
-140 -120 -100 -80 -60 -40 -20 0 20 40 60 80 100 120 140

1045

Table 1: Characteristics of the models, including simulation time slice, spatial resolution, simulated gas species and associated bibliographic references (from Lamarque et al., 2013 and Young et al. 2013). Black carbon (BC), Organic carbon (OC), Secondary Organic Aerosols (SOA), Dimethylsulfide (DMS), Chemistry Climate Model (CCM), Chemistry Transport Model (CTM), Chemistry-General Circulation Model (CGCM).

Models	**Type**	**Simulation length**	**Resolution (lat/lon)**	**Number of vertical pressure levels & top level**	**Species simulated**	**References**
CESM-CAM	CCM	2000-2009 and 2100-2109	1.875/2.5	26 levels 3.5 hPa	**16 gas species**; constant present-day isoprene, soil NOx, DMS and volcanic sulfur, oceanic CO.	Lamarque et al., 2012
GFDL-AM3	CCM	2001-2010 and 2101-2110	2.0/2.5	48 levels 0.017 hPa	**81 gas species**; SOx, BC, OC, SOA, NH_3, NO_3; constant pre-industrial soil NOx; constant present-day soil and oceanic CO, and biogenic VOC; climate-sensitive dust, sea salt, and DMS.	Donner et al., 2011 Naik et al., 2012
GISS-E2-R	CCM	2000-2004 and 2101-2105	2.0/2.5	40 levels 0.14 hPa	**51 gas species**; interactive sulfate, BC, OC, sea salt, dust, NO_3, SOA, alkenes; constant present-day soil NOx; climate-sensitive dust, sea salt, and DMS; climate-sensitive isoprene based on present-day vegetation.	Lee and Adams, 2011 Shindell et al., 2012
MIROC-CHEM	CCM	2000-2010 and 2100-2104	2.8/2.8	80 levels 0.003 hPa	**58 gas species**; SO_4, BC, OC; constant present-day VOCs, soil-NOx, oceanic-CO; climate-sensitive dust, sea salt and DMS.	Watanabe et al., 2011
MOCAGE	CTM	2000-2003 and 2100-2103	2.0/2.0	47 levels 6.9 hPa	**110 gas species**; constant present-day isoprene, other VOCs, oceanic CO and soil NOx.	Josse et al., 2004 Krinner et al., 2005 Teyssèdre et al., 2007
UM-CAM	CGCM	2000-2005 and 2094-2099	2.50/3.75	19 levels 4.6 hPa	**60 gas species**; constant present-day biogenic isoprene, soil NOx, biogenic and oceanic CO.	Zeng et al., 2008, 2010

Table 2a: Annual total emissions of CO (Tg CO/year), NMVOCs (Tg C/year), NOx (Tg N/year, including lightning and soil NOx), total lightning NOx emissions (LNOx) and global atmospheric methane (CH_4) burden (Tg) for the historical simulations in each model (from Young et al., 2013 and * from Voulgarakis et al., 2013).

Models	Historical				
	CO	* CH_4	NMVOCs	NOx	*LNOx
CESM-CAM	1248	4902	429	50.0	4.2
GFDL-AM3	1246	4809	830	46.2	4.4
GISS-E2-R	1070	4793	830	48.6	7.7
MIROC-CHEM	1064	4805	833	57.3	9.7
MOCAGE	1168	4678	1059	47.9	5.2
UM-CAM	1148	4879	535	49.2	5.1

Table 2b: Simulated percentage (%) changes in total emissions of CO, NMVOCs, NOx (including lightning and soil NOx), total lightning NOx emissions (LNOx) and global atmospheric CH_4 burden for each model between 2100 and historical simulation for RCPs (from Young et al., 2013 and *Voulgarakis et al., 2013). The last row shows means and standard deviations (SD). Missing or not available data are identified (n.a).

Models	RCP2.6 scenario					RCP4.5 scenario					RCP8.5 scenario				
	CO	VOCs	NOx	*LNOx	*CH_4	CO	VOCs	NOx	*LNOx	*CH_4	CO	VOCs	NOx	*LNOx	*CH_4
CESM-CAM	- 36.7	0	- 52.8	+ 7.1	- 27.1	n.a	n.a	n.a	n.a	n.a	- 30.1	0	- 33.0	+ 29.7	+ 112.1
GFDL-AM3	- 36.9	- 5.0	- 47.0	+ 12.6	- 27.9	- 47.4	- 3.6	- 41.5	+ 23.5	- 9.3	- 30.3	- 1.9	- 22.4	+ 38.2	+ 116.1
GISS-E2-R	- 42.8	+ 0.5	- 44.2	+ 3.8	- 21.0	- 54.9	+ 6.9	- 39.2	+ 12.2	+ 4.6	- 35.1	+ 19.8	- 20.0	+ 26.2	+ 152.7
MIROC-CHEM	- 43.1	- 7.1	- 36.0	+ 7.5	- 28.2	n.a	n.a	n.a	n.a	n.a	- 35.4	- 3.4	- 6.9	+ 38.0	+ 116.0
MOCAGE	- 39.4	- 6.5	- 45.7	+ 5.2	- 28.8	n.a	n.a	n.a	n.a	n.a	- 32.3	- 2.8	- 22.9	+ 19.9	+ 113.4
UM-CAM	- 39.0	- 11.3	- 40.6	+ 8.1	- 27.9	- 50.4	- 9.2	- 36.0	+ 17.5	- 8.7	- 32.0	- 4.2	- 17.2	+ 43.6	+ 112.1
Mean ± SD	- 39.7 ± 2.2	- 4.9 ± 4.9	- 44.4 ± 4.3	+ 7.4 ± 2.0	- 26.8 ± 3.7	- 50.9 ± 3.2	- 2.0 ± 11.4	- 38.9 ± 2.3	+ 17.7 ± 3.7	- 4.5 ± 9.4	- 32.5 ± 1.8	+ 1.3 ± 11.6	- 20.4 ± 7.0	+ 32.6 ± 10.8	+ 120.4 ± 19.5

Table 3a: Global and hemispheric (averaged over the land points of ~~over~~ the domain) mean annual-average surface ozone concentrations (in ppb) and mean AOT40 (in ppm.h) for the historical simulations in each model (North and South Hemisphere, i.e NH and SH). The last row shows means and standard deviations (SD).

Models	Ozone conc. global	Ozone conc. SH	Ozone conc. NH	AOT40 global	AOT40 SH	AOT40 NH
CESM-CAM	31.3	20.9	36.4	12.8	0.2	18.9
GFDL-AM3	38.6	30.6	42.9	21.8	4.7	30.8
GISS-E2-R	35.8	22.3	42.3	26.0	3.6	36.8
MIROC-CHEM	27.9	20.4	31.4	7.3	1.9	9.8
MOCAGE	32.9	21.5	38.3	22.9	3.5	31.8
UM-CAM	31.3	21.4	36.0	14.4	1.3	20.6
Mean ± SD	33.0 ± 3.8	22.9 ± 3.8	37.9 ± 4.3	17.5 ± 7.2	2.5 ± 1.7	24.8 ± 10.1

Table 3b: Simulated percentage (%) changes in global and hemispheric mean annual-average surface ozone concentrations~~-~~ (over the land points of the domain) and in global mean stratospheric ozone column (* from Voulgarakis et al., 2013) for each model between 2100 and historical simulation for RCPs (North and South Hemisphere, i.e NH and SH). The last row shows means and standard deviations (SD). Missing or not available data are identified (n.a).

Models	Surface ozone mean concentrations									* Stratospheric ozone		
	RCP2.6 global	RCP2.6 SH	RCP2.6 NH	RCP4.5 global	RCP4.5 SH	RCP4.5 NH	RCP8.5 global	RCP8.5 SH	RCP8.5 NH	RCP2.6 global	RCP4.5 global	RCP8.5 global
CESM-CAM	- 29.1	- 20.6	- 31.3	n.a	n.a	n.a	+ 21.9	+ 22.5	+ 20.5	n.a	n.a	+ 5.3
GFDL-AM3	- 20.5	- 10.8	- 24.5	- 11.7	- 6.9	- 13.5	+ 15.5	+ 18.6	+ 14.5	+ 3.3	+ 3.9	+ 8.4
GISS-E2-R	- 23.5	- 5.8	- 27.9	- 20.4	- 6.3	- 23.9	+ 7.0	+ 19.3	+ 3.8	+ 8.0	+ 8.8	+ 15.1
MIROC-CHEM	- 23.3	- 12.3	- 26.8	n.a	n.a	n.a	+ 3.9	+ 10.3	+ 2.2	+ 2.6	n.a	+ 4.2
MOCAGE	- 12.8	+ 7.4	- 18.5	- 1.8	+ 17.7	- 7.0	+ 23.1	+ 40.4	+ 16.7	+ 19.9	n.a	+ 23.6
UM-CAM	- 17.3	- 4.7	- 21.1	- 8.3	+ 0.9	- 10.8	+ 14.4	+ 24.3	+ 11.4	+ 6.7	+ 6.9	+ 7.4
Mean ± SD	- 21.1 ± 5.6	- 7.8 ± 9.4	- 25.0 ± 4.7	- 10.5 ± 7.7	+ 1.4 ± 11.5	- 13.8 ± 7.2	+ 13.8 ± 7.1	+ 22.6 ± 10.0	+ 11.5 ± 7.3	+ 8.1 ± 7.0	+ 6.5 ± 2.5	+ 10.7 ± 7.4

Table 3c: Simulated percentage (%) changes in global and hemispheric mean AOT40 (over the land points of the domain) for each model between 2100 and historical simulation for RCPs (North and South Hemisphere, i.e NH and SH). Missing or not available data are identified (n.a).

Models	AOT40								
	RCP2.6 global	**RCP2.6 SH**	**RCP2.6 NH**	**RCP4.5 global**	**RCP4.5 SH**	**RCP4.5 NH**	**RCP8.5 global**	**RCP8.5 SH**	**RCP8.5 NH**
CESM-CAM	- 96.9	- 99.9	- 96.8	n.a	n.a	n.a	+ 138.3	+ 150.0	+ 134.9
GFDL-AM3	- 75.2	- 25.5	- 78.9	- 53.2	- 36.2	- 54.5	+ 96.3	+ 242.5	+ 85.1
GISS-E2-R	- 78.1	- 13.9	- 81.2	- 75.0	- 27.8	- 77.2	+ 22.3	+ 83.3	+ 19.5
MIROC-CHEM	- 74.0	- 10.5	- 80.6	n.a	n.a	n.a	+ 20.5	+ 78.9	+ 16.3
MOCAGE	- 53.7	+ 68.6	- 59.7	- 17.5	+ 202.9	- 28.3	+ 85.1	+ 448.6	+ 67.0
UM-CAM	- 73.6	+ 92.3	- 76.7	- 52.8	+7.7	- 54.8	+ 49.3	+ 176.9	+ 45.1
Mean ± SD	- 75.2 ± 13.7	+ 1.9 ± 69.5	- 79.0 ± 11.8	- 49.6 ± 23.8	+ 36.6 ± 112.4	- 53.7 ± 20.0	+ 68.6 ± 46.3	+ 196.7 ± 137.7	+ 61.3 ± 44.8

Table 3d: Simulated percentage (%) changes in potential O_3 impact on vegetation (IO3, over the land points of the domain) for each model between 2100 and historical simulation for RCPs (North and South Hemisphere, i.e NH and SH).Missing or not available data are identified (n.a).

Models	Risk factor IO3								
	RCP2.6 global	**RCP2.6 SH**	**RCP2.6 NH**	**RCP4.5 global**	**RCP4.5 SH**	**RCP4.5 NH**	**RCP8.5 global**	**RCP8.5 SH**	**RCP8.5 NH**
CESM-CAM	- 97.2	- 91.8	-97.5	n.a	n.a	n.a	+ 129.6	+146.8	+127.5
GFDL-AM3	- 69.4	- 49.1	- 74.8	- 50.1	- 61.1	- 47.2	+ 91.9	+95.5	+90.4
GISS-E2-R	- 66.1	- 20.7	- 74.3	- 71.7	- 53.3	- 74.6	+ 21.5	+56.6	+14.2
MIROC-CHEM	- 41.4	- 18.9	- 51.9	n.a	n.a	n.a	+ 41.0	+103.8	+25.5
MOCAGE	- 46.6	-22.8	- 51.4	- 7.0	- 38.0	- 1.0	+ 77.7	+68.2	+80.0
UM-CAM	- 45.8	- 9.2	- 71.3	- 59.5	+ 2.0	- 69.0	+ 61.3	+84.2	+56.0
Mean ± SD	- 61.1 ± 21.1	- 35.5 ± 30.7	- 70.2 ± 17.2	- 47.1 ± 28.1	- 37.6 ± 28.1	- 47.9 ± 33.4	+ 70.5 ± 38.4	+ 92.5 ± 31.7	+ 65.6 ± 42.4